International Geology Review, Vol. 49, 2007, p. 454–478.

Ultrahigh-Pressure Mineral Assemblages in Zircons from the Surface to 5158 m Depth in Cores of the Main Drill Hole, Chinese Continental Scientific Drilling Project, Southwestern Sulu Belt, China

FULAI LIU,[1] ZHIQIN XU,
Institute of Geology, Chinese Academy of Geological Sciences, Beijing 100037, China

J. G. LIOU,
Department of Geological and Environmental Sciences, Stanford University, Stanford, California 94305

HAILIANG DONG,
Department of Geology, Miami University, Oxford, Ohio 45056

AND HUAIMIN XUE
Institute of Geology, Chinese Academy of Geological Sciences, Beijing 100037, China

Abstract

The 5158 m deep main hole of the Chinese Continental Scientific Drilling Project (CCSD-MH) at Maobei, southwestern Sulu Belt, penetrated five major lithologic units: eclogite, amphibolite ± retrograde eclogite, ultramafic rock, paragneiss, and orthogneiss. All analyzed samples are overprinted to various extents by amphibolite-facies retrograde metamorphism. Ultrahigh-pressure (UHP) index minerals are preserved as inclusions in zircons separated from 137 core samples. These index assemblages include: Coe + Phe + Grt from Grt-Ep-Bt paragneiss; Coe + Jd + Grt + Ap, Coe + Jd + Phe + Ap and Coe + Grt + Jd + Phe from Grt-Ep-Hbl paragneiss; Coe + Phe, Coe + Ky + Ap, and Coe + Ky + Ttn from orthogneiss; and Coe + Grt + Omp, Coe + Grt + Phe, Coe + Omp + Rt, and Coe + Grt + Omp + Phe from Bt-Ep amphibolite and other retrograde eclogites. The common occurrences of these UHP assemblages throughout the section indicate that the drill hole did not penetrate through the UHP tectonic slice. All of the UHP mineral assemblages, whether from retrograde ecologites or from the surrounding gneisses, record similar metamorphic conditions of 773–843°C and 3.2–4.0 GPa. Zircons separated from surface samples and cores from other shallow holes in the area also contain similar coesite-bearing UHP mineral inclusions. This widespread occurrence of UHP assemblages in the southwestern Sulu area suggests that voluminous continental materials were subducted and metamorphosed at mantle depths > 100 km, and then were rapidly exhumed to crustal levels.

Introduction

ZIRCON IS AN excellent container of ultrahigh-pressure minerals because it is petrologically stable and chemically resistant over a wide P-T range (Chopin and Sobolev, 1995; Katayama et al., 2000; Ye et al., 2000; Liu et al., 2002). In the Sulu-Dabie terrane, the presence of coesite and diamond in eclogites (Enami and Zang, 1989; Okay et al., 1989; Wang et al., 1989; Xu et al., 1992, 2005), and of coesite inclusions in zircons from eclogite and adjacent country rocks (Tabata et al., 1998; Ye et al., 2000) indicate widespread UHP metamorphism in the region. However, because early studies of the Sulu-Dabie UHP terrane focused mainly on spatially discontinuous outcrops (Tabata et al., 1998; Ye et al., 2000; J. B. Liu et al., 2001), it was not clear whether the entire lithologic assemblage had experienced *in situ* UHP metamorphism, or whether the UHP rocks were foreign blocks incorporated in lower-grade gneisses (Wang and Liou, 1991; Okay and Sengör, 1992; Zhang et al., 1995; Hacker et al., 1998; Liou et al., 2000). From systematic studies of mineral inclusions in zircons from both eclogite and

[1]Corresponding author; email: liufulai@ccsd.cn

eclogite-hosting country rock (F. L. Liu et al., 2001, 2002, 2003) were able to confirm an *in situ* metamorphic model. However, little was known about the 3-D distribution of the UHP rocks until samples were available from the CCSD main drill hole, which was completed in 2005.

The CCSD main drill hole (with a total depth of 5158 m) recovered continuous cores that allowed identification of vertical variations in UHP mineral assemblages. Zircons were separated from all the UHP lithologies, including eclogite, retrograde eclogite, amphibolite, paragneiss, and orthogneiss, and their mineral inclusions were identified and analyzed using a Laser Raman spectroscope and an electron microprobe. Cathodoluminescence (CL) images of the zircons were used to constrain zircon growth zones.

In this paper, we focus on zircons collected from the CCSD-MH eclogites and their host rocks in order to: (1) identify index UHP mineral inclusions and related UHP assemblages in zircons; (2) determine the distribution of UHP and non-UHP mineral inclusions in different zircon domains, and clarify the parageneses of the minerals in zoned zircons; (3) trace vertical change of index UHP inclusions in zircons with depth; (4) examine the genetic relationship between UHP mineral assemblages and host rocks; (5) directly measure the thickness of the subducted slab; and (6) use these data to discuss the metamorphic evolution of the Sulu UHP terrane. Mineral abbreviations in this work follow Kretz (1983).

Geological Setting

The Sulu high-pressure (HP) and ultrahigh-pressure metamorphic terrane extends NE-SW for ~750 km and is 180 km wide (Xu et al., 2006). It is separated from the Sino-Korean craton to the northwest by the Yantai-Qingdao-Wulian fault (YQWF), and the Yangtze craton to the southeast by the Jiashan-Xiangshui fault (JXF) (Fig. 1). Field observations and petrologic data suggest that the southwestern Sulu terrane is composed primarily of four lithological units: (1) orthogneiss (Unit I); (2) supracrustal rock (Unit II); (3) kyanite-bearing quartzite + marble (Unit III); and (4) paragneiss-schist (Unit IV). All of these rocks show evidence of retrograde amphibolite- to greenschist-facies metamorphism, and some are locally intruded by Cretaceous granites. These four units are separated from one another by ductile shear zones (Xu et al., 2003, 2006). Coesite-bearing UHP mineral assemblages occur as inclusions in zircons from various amphibolite-facies metamorphic rocks in Units I and II (Fig. 1). In contrast, zircon in the amphibolites and greenschists of Units III and IV mostly contain HP assemblages, such as Arg + Phe + Qtz, Phe + Qtz + Ap, and Ky + Phe + Qtz.

Unit I, ~20 km wide, contains mostly coesite-bearing granitic gneiss and subordinate amounts of supracrustal rock intercalated with eclogite lenses, ultramafic blocks, and marble layers. This unit was intruded by post-orogenic Cretaceous granite (Fig. 1). Unit II is ~20–30 km wide and consists mainly of UHP supracrustal rocks intercalated with eclogitic and ultramafic lenses. The supracrustal rocks include coesite-bearing paragneiss, kyanite quartzite, jadeite quartzite, mica schist, and amphibolite. Several small metamorphosed Neoproterozoic granitic bodies intrude the supracrustal rocks. The CCSD-MH and two pre-pilot drill holes (CCSD-PP1 and -PP2) were all spudded in this unit near Maobei village (Fig. 1). Unit III is 5–12 km wide and composed mainly of kyanite-bearing quartzite, kyanite-bearing phengite-quartz schist, and apatite-bearing marble. This unit was recently recognized by the presence of OH-topaz in kyanite-bearing quartzite in Hanshan (Zhang et al., 2002). Petrologic studies show that the metamorphic rocks of this unit experienced HP metamorphism, and were later overprinted by blueschist-facies retrograde metamorphism (Xu et al., 2006). The topaz in the kyanite-bearing quartzite formed at temperatures of 500–600°C and pressures of 1.5–2.5 GPa (Zhang et al., 2002). Unit IV is ~40 km wide and consists mainly of paragneiss with variable amounts of biotite, epidote, and amphibole, phengite-bearing quartz schist, and rare blueschist (Zhang et al., 1995; Xu et al., 2003). The protoliths for this unit were mostly sedimentary rocks, with minor mafic volcanic material (Xu et al., 2006). The textures of these rocks and thermobarometric studies suggest early blueschist-facies metamorphism at 300–360°C and 0.70-0.85 GPa, followed by retrograde greenschist facies metamorphism at 350-410°C and 0.2–0.4 GPa (Xu et al., 2006).

Petrologic Characteristics of Cores from the CCSD-MH

The CCSD-MH is located at 34°24' N, 118°40' E, about 17 km southwest of Donghai (Fig. 1). The drillhole, completed in 2005, penetrated to a depth

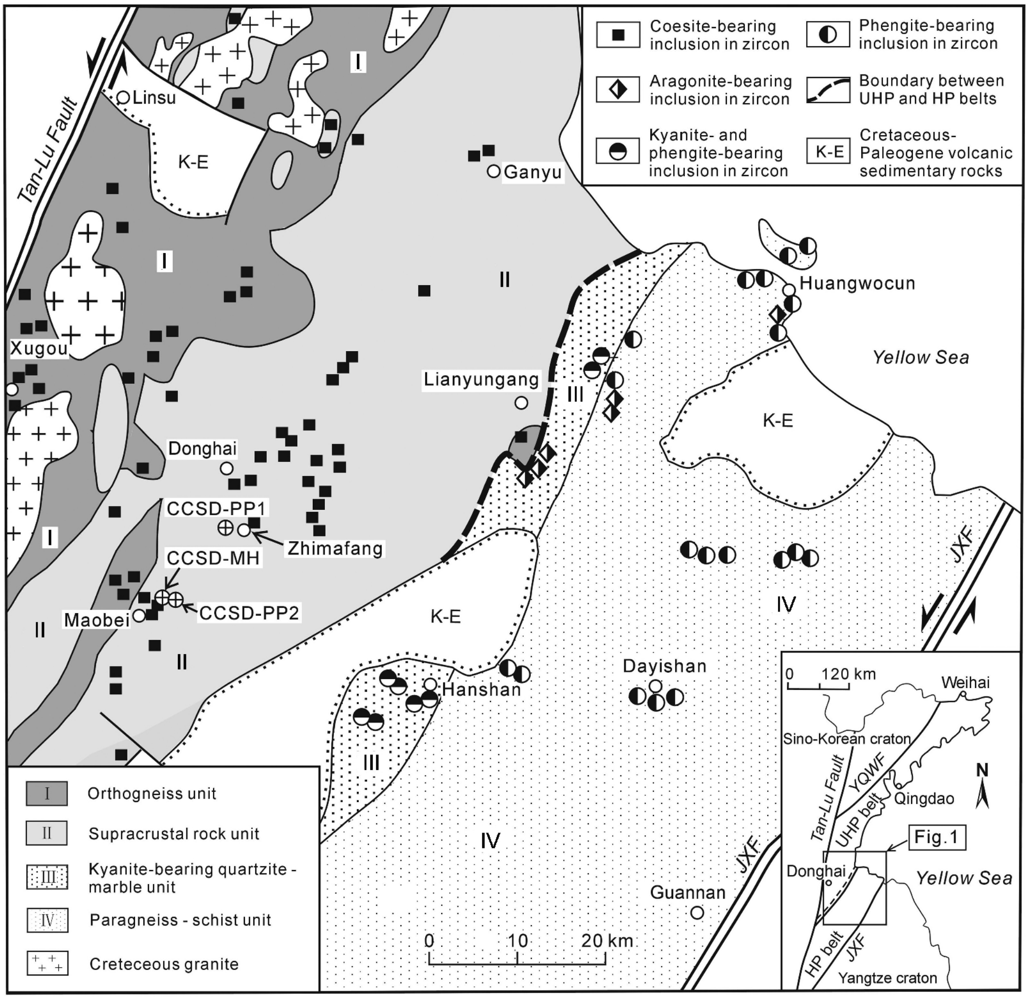

FIG. 1. Tectonic sketch map of the southwestern Sulu terrane, showing major lithotectonic units and the locations of zircon samples. Abbreviations: YQWF = Yantai-Qingdao-Wulian fault; JXF = Jiashan-Xiangshui fault.

of 5158 m and sampled five major lithologic units with 85% core recovery. In general, the rocks all have a uniform attitude, with a NE-SW–trending foliation that dips 25–35° SE, and a SE-plunging stretching lineation (Xu et al., 2004). A lithological profile of the main hole and the locations of recognized coesite-bearing cores are shown in Figure 2. The general petrological features of representative core samples are described below.

Eclogite

Eclogite has a cumulative thickness of about 649 m in the CCSD-MH and constitutes 12.6 % of the recovered core. It is most abundant in the upper 2000 m of the section, where it forms relatively thick layers containing thin bands of paragneiss, orthogneiss, and amphibolite-facies retrograde eclogite (Fig. 2) (Liu et al., 2004b). In the lower 3000 m, it forms thin layers, 5–20 m thick, intercalated within paragneiss, orthogneiss, and ultramafic rocks. The eclogites consist mainly of garnet and omphacite, with accessory quartz, rutile, phengite, kyanite, and zircon. Inclusions of zircon are common in both garnet and omphacite. Three types of eclogite are recognized based on the abundance of accessory minerals; rutile-and quartz-bearing eclogite, rutile-and phengite-bearing eclogite, and rutile-bearing eclogite. The rutile-and quartz-bearing eclogite

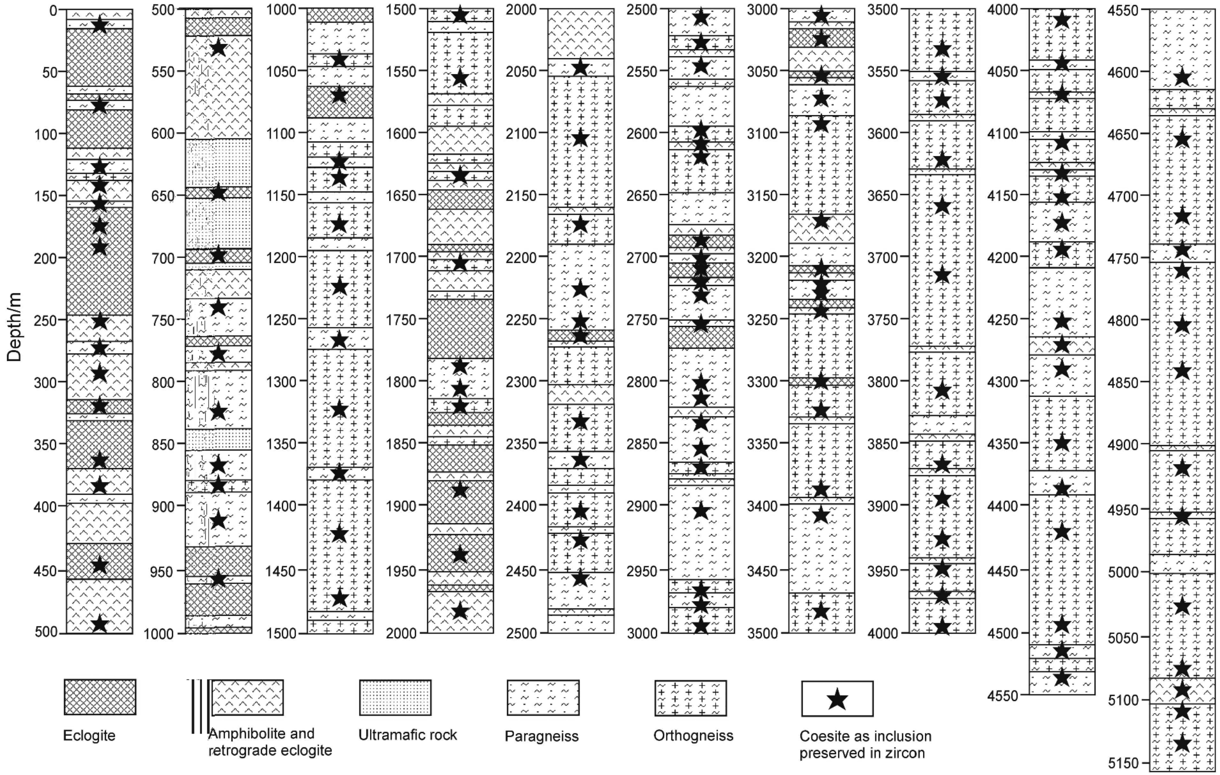

FIG. 2. Simplified lithologic profile of the main drill hole of Chinese Continental Scientific Drilling Porject in Maobei, southwestern Donghai. This hole recovered mainly eclogite, retrograde eclogite, amphibolite, paragneiss, orthogneiss, and ultramafic rock. Locations of coesite-bearing zircon separated from core samples for the present study are shown as stars.

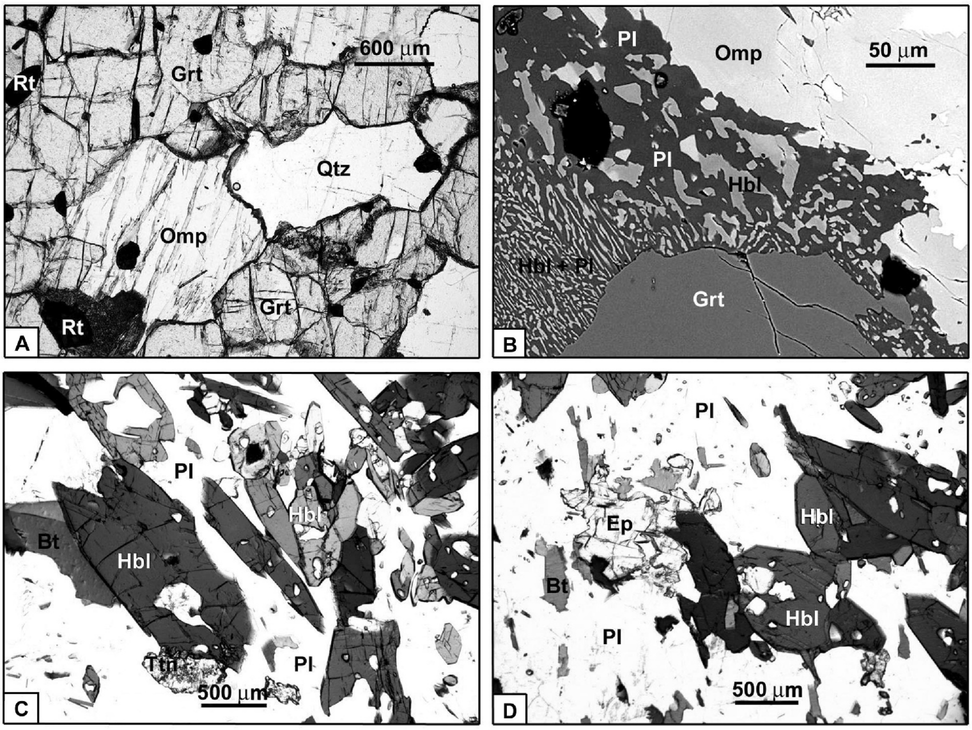

FIG. 3. Photomicrographs showing texture and mineral assemblages of rutile+quartz-bearing eclogite (sample B42, 174.1 m depth) and epidote-bearing amphibolite (sample B25, 142.6 m depth). A. Rutile + quartz-bearing eclogite consists of garnet, omphacite, quartz, and rutile (plane-polarized light). B. Garnet and omphacite in rutile + quartz-bearing eclogite are partly replaced by hornblende and plagioclase (backscattered electron image). C and D. Epidote-bearing amphibolite consists of hornblende, plagioclase, and epidote, with accessory biotite and titanite (plane-polarized light).

contains a Grt + Omp + Rt + Qtz assemblage (Fig. 3A); some of the Grt and Omp crystals are partly replaced by Hbl + Pl (Fig. 3B). Although coesite was not found in the matrix, quartz pseudomorphs after coesite are common inclusions in the garnets.

Amphibolite and retrograde eclogite

Amphibolite and retrograde eclogite have a cumulative thickness of about 706 m and make up 13.6 % of the recovered core. They commonly occur adjacent to unaltered eclogite or as layers, 5 to 25 m thick, in the gneissic rocks (Fig. 2). Boundaries between fresh eclogite and amphibolite are invariably transitional, ranging from eclogite to amphibolitized eclogite (retrograde eclogite), through garnet-bearing amphibolite to epidote-bearing amphibolite, strongly suggesting that the amphibolites are retrograded from the eclogites (Liu et al., 2003). The epidote-bearing amphibolite consists mainly of Hbl + Pl + Ep, with trace amounts of Bt, Ttn, and Qtz (Figs. 3C and 3D). No coesite inclusions or coesite pseudomorphs were found in the matrix minerals.

Paragneiss

Paragneiss makes up about 25.3% of the recovered core and has a cumulative thickness of 1305 m. It occurs as layers ranging from 20 to 150 m in thickness, and occurs mainly in the interval of 736–4616 m (Fig. 2). In the core, the paragneiss displays a sharp contact with the other metamorphic rocks (e. g., eclogite, orthogneiss, amphibolite, and ultramafic rock). The paragneisses are grey and contain distinct layers of different mineral assemblages. Because all of the paragneiss has been retrograded, it contains only amphibolite-facies mineral assemblages (Figs. 4 and 5); no index UHP minerals were identified in the matrix. Based on their mineralogy, the paragneisses are subdivided into three main types: (1) garnet-epidote-biotite-K-feldspar gneiss (Figs. 4A and 4B), which contains zircon inclusions

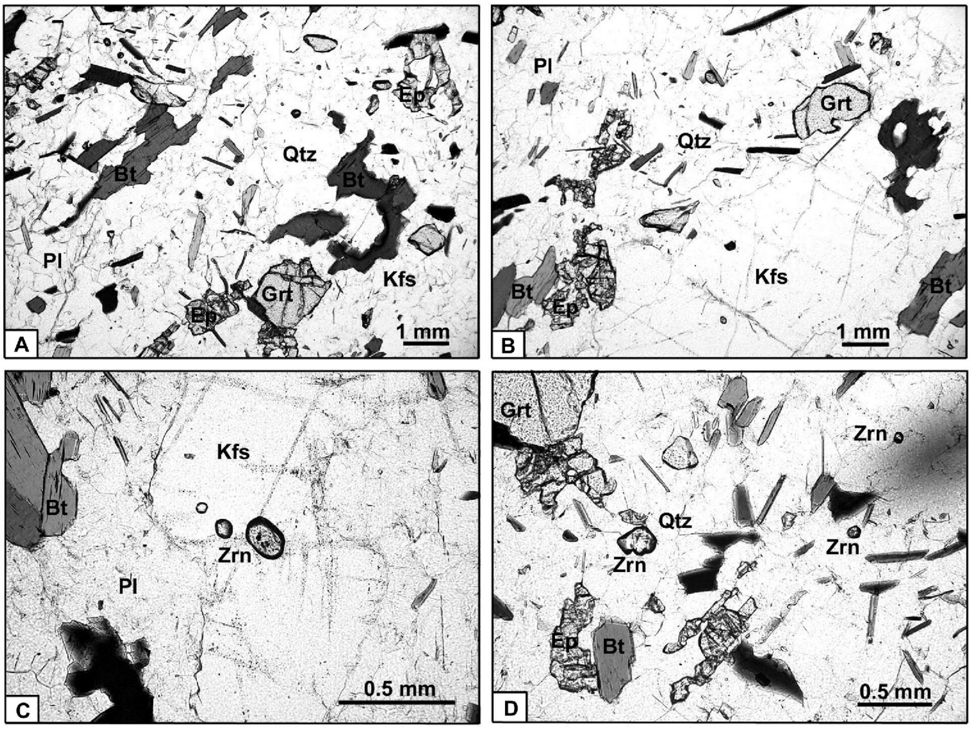

FIG. 4. Photomicrographs (plane-polarized light) showing texture and mineral assemblages of garnet-epidote-biotite–K-feldspar gneiss (sample B525, 958.7 m depth). A and B. Garnet-epidote-biotite–K-feldspar gneiss consists of garnet, epidote, biotite, plagioclase, K-feldspar, and quartz. C. Zircons as inclusions are preserved in K-feldspar. D. Zircons as inclusions are common in quartz.

in K-feldspar and quartz (Figs. 4C and 4D); (2) garnet-biotite-hornblende gneiss (Fig. 5), with rare inclusions of ilmenite, titanite, and zircon in the plagioclase (Figs. 5B and 5C) and quartz (Fig. 5D); and (3) epidote-phengite-biotite–K-feldspar gneiss that shows partial replacement of phengite by biotite and has zircon inclusions in K-feldspar, plagioclase, and quartz.

Orthogneiss

A few large orthogneiss layers occur in the intervals of 1113–1596 m, 2055–2182 m, 2272–2453 m, 3088–3397 m, 3470–4157 m, 4318–4530 m, and 4616–5158 m. Much thinner layers, 0.5 to 25 m thick, are intercalated with eclogite, retrograde eclogite, and paragneiss elsewhere in the core (Fig. 2). The orthogneiss has a cumulative thickness of about 2428 m and makes up 47.1% of the core. All of these rocks have undergone amphibolite-facies retrograde metamorphism (Liu et al., 2004b). The orthogneisses are light-colored, medium- to coarse-grained, and consist mainly of Kfs + Pl + Qtz, with accessory Ep, Bt, Hbl, Grt, Phe, and Mag. Five major varieties are recognized: biotite-bearing granitic gneiss, hornblende-bearing granitic gneiss, garnet-bearing granitic gneiss, hornblende- and biotite-bearing granitic gneiss, and epidote- and biotite-bearing granitic gneiss. The biotite-bearing granitic gneiss, which is the most common metamorphic rock in the CCSD-MH, consists mainly of Kfs + Qtz + Bt + Mag ± Pl (Figs. 6A and 6B). Zircon inclusions occur in both quartz and K-feldspar (Figs. 6C and 6D). Epidote + biotite–bearing granitic gneiss is also common, and consists mainly of Kfs + Pl + Qtz + Ep + Bt ± Hbl (Figs. 7A and 7B). Zircon occurs as an intergranular mineral between K-feldspar and quartz (Fig. 7C) or as inclusions in plagioclase and K-feldspar (Fig. 7D).

Ultramafic rocks

Two ultramafic layers, composed of garnet lherzolite and harzburgite, occur at depths of 608–683 m and 839–852 m (Liu et al., 2004b; Fig. 2). They have a cumulative thickness of about 69 m and

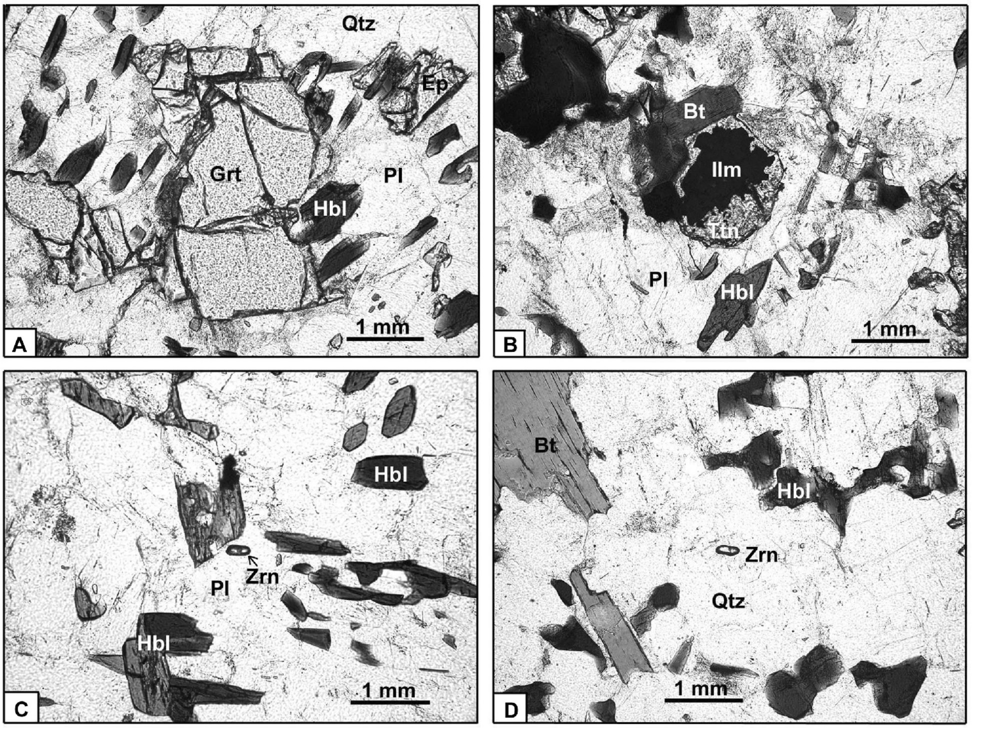

FIG. 5. Photomicrographs (plane-polarized light) showing texture and mineral assemblages of garnet-biotite-hornblende paragneiss (sample B13, 124.6 m depth). A and B. Garnet-biotite-hornblende paragneiss consists of garnet, biotite, epidote, hornblende, plagioclase, quartz, ilmenite, and titanite. Garnet and ilmenite is partly replaced by hornblende and titanite, respectively. C. Zircon inclusions are preserved in plagioclase. D. Zircon inclusions are common in quartz.

make up 1.4 % of the recovered core. Although some fresh minerals are present, the rocks are intensely serpentinized and chloritized, especially near the contacts with amphibolite, eclogite, and paragneiss.

Techniques for Analysis of Mineral Inclusions in Zircon

Zircons were separated from 240 core samples from the CCSD-MH, including 17 eclogites, 17 amphibolites, 47 paragneisses, and 159 orthogneisses. After crushing and sieving approximately 2.0–5.0 kg of each sample, zircons were separated by magnetic and heavy liquid techniques, and then hand-picked from the residue. Between 150 and 700 zircon grains, ranging from 50 to 400 μm in diameter, were recovered from each sample. These grains were mounted and polished in 25 mm epoxy discs. Discrete inclusions in zircons were identified using a RENISHOW-1000 laser Raman spectroscope with the 514.5 nm line of an Ar-ion laser, at the Key laboratory for Continental Dynamics, Ministry of Land and Resources of China. Laser Raman spectroscopy is a particularly useful, nondestructive method with which to analyze mineral inclusions preserved in zircon grains. The relationships between the host zircon and the inclusions were observed by optical microscope and by cathodoluminescence (CL) image analysis at the Institute of Mineral Resources, Chinese Academy of Geological Sciences. Representative compositions of the inclusions were analyzed using a JEOL JXA-8100 electron probe micro-analyzer at Peking University. Analytical conditions were optimized for standard silicates and oxides at 15 kV accelerating voltage, with 20 nA beam current and a ~1 μm beam spot for all the elements. The locations of coesite-bearing zircon cores are shown in Figure 2.

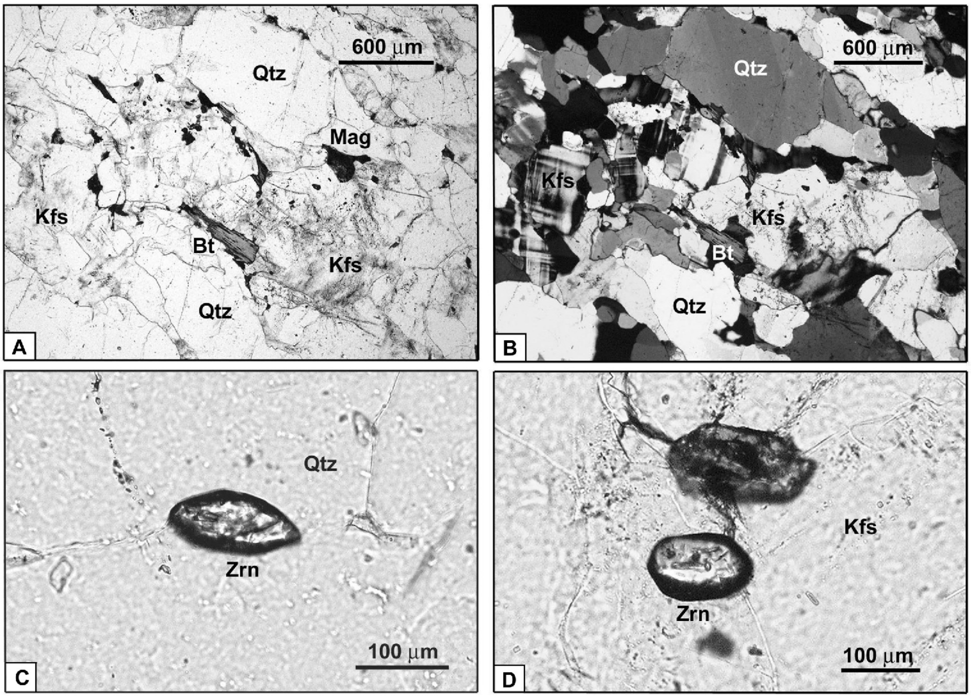

FIG. 6. Photomicrographs showing texture and mineral assemblages of biotite-bearing granitic gneiss (sample B1811, 3623.6 m depth). A. Biotite-bearing granitic gneiss consists of biotite, K-feldspar, quartz, and magnetite (plane-polarized light). B. Cross-polarized light image of Figure 6A. C. Zircon inclusions are preserved in quartz (plane-polarized light). D. Zircon inclusions are identified in K-feldspar (plane-polarized light).

Mineral Inclusions in Zircon Separates from Eclogite

Zircon separates from 17 eclogite cores contain inclusions of coesite, garnet, omphacite, and phengite or muscovite, quartz, calcite, and apatite (Fig. 8, Table 1). Two groups of zircon crystals are recognized in the rutile- and quartz-bearing eclogite (B42, 174.1 m depth; Figs. 3A and 3B). The first group consists of light yellow grains with dusty cores and clear, colorless mantles and rims (Figs. 8A and 8C). Cathodoluminescence (CL) images of these grains show low-luminescent cores, bright-luminescent mantles, and narrow low-luminescent rims (Figs. 8B and 8D). Most of the grains have prismatic cores with well-developed oscillatory zoning, suggesting magmatic crystallization. Most of the cores contain low-P inclusions such as Qtz + Ms + Ap (Fig. 8A) and Qtz + Cal + Ap (Fig. 8C); only a few contain Di + Ap (Table 1). Coesite (Fig. 8C) and Coe + Grt (Fig. 8A) inclusions are preserved in the mantles, whereas the rims contain Qtz or are inclusion-free (Figs. 8A and 8B). The inclusion distribution in these grains suggests that: (a) the euhedral zircon cores with diopside inclusions are inherited igneous grains; (b) the mantles are UHP metamorphic overgrowths; and (c) the rims formed by retrograde metamorphism.

The second group of zircons consists of small, colorless grains with bright luminescent cores and mantles, and narrow low luminescent rims (Figs. 8E, 8F, 8G, and 8H). UHP inclusions, including Coe + Grt + Omp (Fig. 8E) and Coe + Phe + Ap (Fig. 8G) were identified in all of these zones, suggesting either that these grains formed during UHP metamorphism, or that the observed sections do not cut through any inherited cores.

Mineral Inclusions in Zircon Separates from Amphibolite

Zircons separated from 17 amphibolite cores contain abundant mineral inclusions, including coesite, garnet, omphacite, phengite, rutile, quartz, calcite, and apatite (Figs. 9A, 9C and 9E) in different

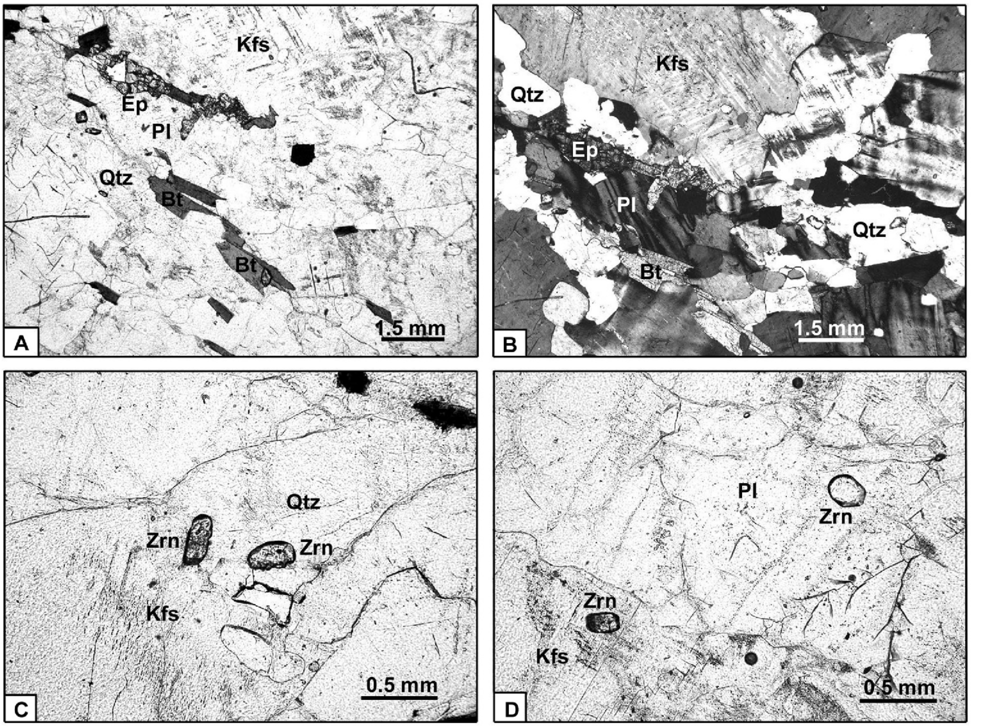

FIG. 7. Photomicrographs showing texture and mineral assemblages of epidote- and biotite-bearing granitic gneiss (sample B2487, 4809.1 m depth). A. Epidote- and biotite-bearing granitic gneiss consists of epidote, biotite, K-feldspar, plagioclase, and quartz (plane-polarized light). B. Cross-polarized light image of Figure 7A. C. Intergranular zircons are identified between K-feldspar and quartz (plane-polarized light). D. Zircon inclusions are preserved in plagioclase and K-feldspar (plane-polarized light).

domains (Table 1). The CL images reveal pronounced zoning characterized by low-luminescent cores (C), surrounded by bright-luminescent mantles (M), and irregular low-luminescent rims (R) (Figs. 9B, 9D, and 9F). Most cores are prismatic, show well-developed oscillatory zoning, and are igneous in origin. The inherited cores contain low-P inclusions, such as Qtz + Ap (Fig. 9A) and Qtz + Cal + Ap (Figs. 9C and 9E), whereas the mantles have several UHP assemblages: Coe + Grt + Omp (Fig. 9A), Coe + Grt + Phe (Fig. 9C), Coe + Omp + Rt (Fig. 9E), and Coe + Grt + Omp + Phe (Table 1). These UHP assemblages were not found in the matrix of the same amphibolite samples (Figs. 3C and 3D). The UHP assemblages are similar to those in zircons from eclogite (Fig. 8) and in the eclogite matrix (Figs. 3A and 3B). These data indicate that the amphibolites experienced UHP metamorphism, but that their matrix assemblages were replaced by retrograde amphibolite-facies minerals.

Mineral Inclusions in Zircon Separates from Paragneiss

Mineral inclusions were separated from two paragneiss cores, including garnet-epidote-biotite–K-feldspar gneiss (B525, 958.7 m depth) and garnet-biotite-hornblende paragneiss (B13, 124.6 m depth). The separated zircons contain abundant inclusions, including coesite, garnet, jadeite, phengite, quartz, and apatite, but the assemblages vary significantly within individual zircon grains and individual zones (Table 1, Figs. 10 and 11). Coesite inclusions occur in zircons from all the analyzed samples, mostly in the following assemblages: Coe + Phe (Fig. 10A), Coe + Grt (Fig. 10E), Coe + Grt + Jd + Ap (Fig. 11A), Coe + Jd + Phe + Ap (Fig. 11C), Coe + Grt + Ap (Fig. 11E), and Coe + Grt + Jd + Phe (Table 1). Jadeite inclusions occur in zircons from the garnet-biotite-hornblende paragneiss (B13, 124.6 m depth) (Figs. 11A and 11C), but are absent

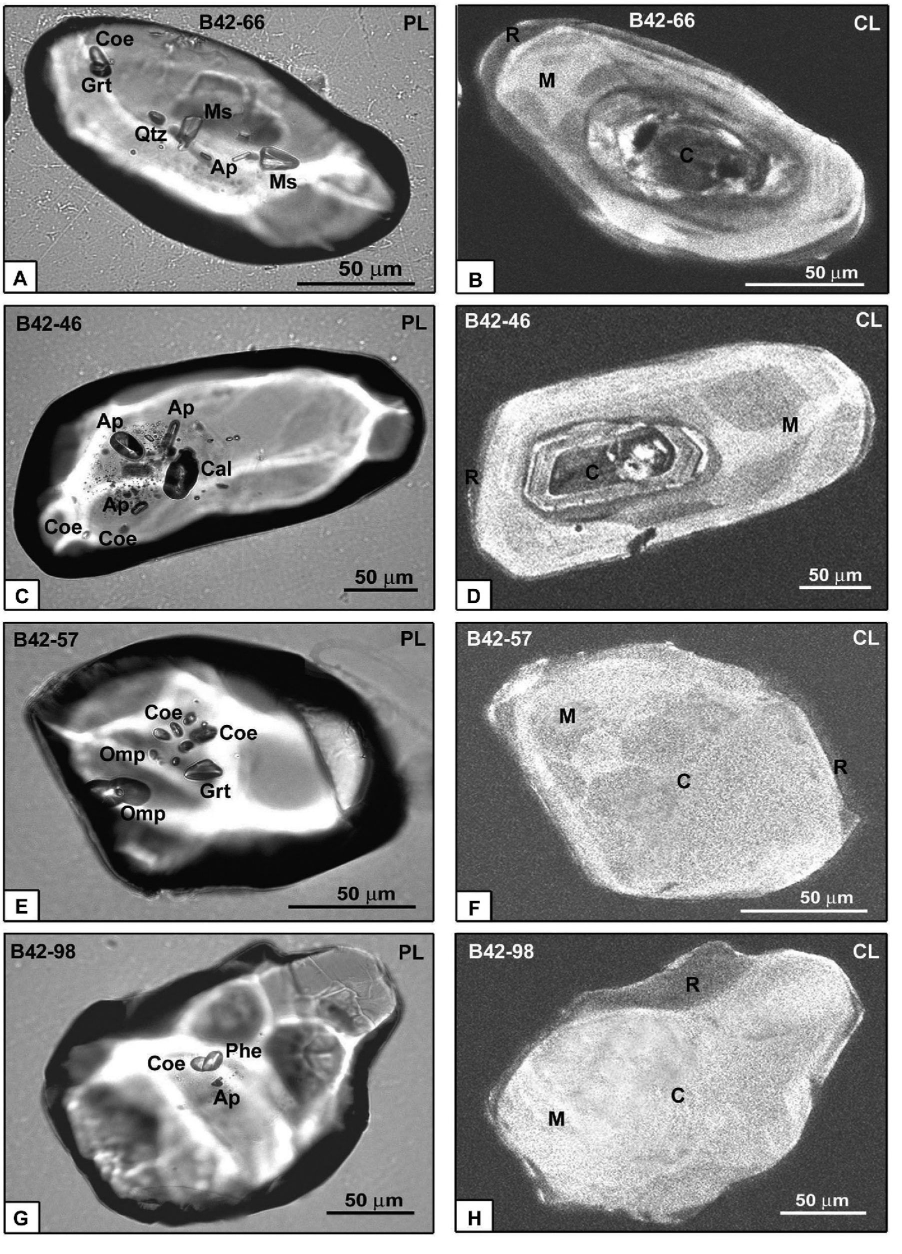

FIG. 8. Plane-polarized light (PL) images of mineral inclusion assemblages and CL images of host zircon from eclogite (sample B42, 174.2 m depth). A. Zircon grain B42-66 shows Qtz + Ms + Ap inclusions in the core, Coe + Grt inclusions in the mantle, and has an inclusion-free rim. B. CL image of the same zircon as in Figure 8A. Abbreviations: C = core; M= mantle; R = rim. C. Zircon grain B42-46 contains Cal + Ap in the core, Coe in the mantle, and has an inclusion-free rim. D. CL image of the same zircon as in Figure 8C. E. Clear zircon grain B42-57 contains inclusions of Coe + Grt + Omp in the core and mantle. F. CL image of the same zircon as in Figure 8E shows bright luminescent core and mantle, and low luminescent rim, with no distinct boundary between core and mantle. G. Clear zircon grain B42-98 contains inclusions of Coe + Phe + Ap in the core and mantle. H. CL image of the same zircon as in Figure 8G shows bright luminescent core and mantle, and low luminescent rim, with no distinct boundary between core and mantle.

TABLE 1. Distribution of Mineral Inclusions in Different Microdomains of Zircons from Eclogite, Amphibolite, Paragneiss, and Orthogneiss Cores in the Main Drill Hole of the Chinese Continental Scientific Drilling Project

Metamorphic rocks	Inherited (Detrital) core	Coesite-bearing overgrowth domain	Outmost rim
Eclogite	Qtz + Ms + Ap Qtz + Cal + Ap Di + Ap	Coe Coe + Grt Coe + Grt + Omp Coe + Phe + Ap Coe + Grt + Omp + Phe	Qtz or mineral inclusion–free
Amphibolite	Qtz + Ap Qtz + Cal + Ap	Coe + Grt + Omp Coe + Grt + Phe Coe + Omp + Rt Coe + Grt + Omp + Phe	Mineral inclusion–free
Grt-Ep-Bt paragneiss	Qtz Qtz + Ap	Coe Coe + Phe Coe + Grt	Qtz or mineral inclusion–free
Grt-Bt-Hbl paragneiss	Qtz + Ap	Coe + Jd + Grt + Ap Coe + Jd + Phe + Ap Coe + Grt + Ap Coe + Grt + Jd + Phe	Mineral inclusion–free
Ep-Bt-bearing orthogneiss	Qtz + Ap Qtz + Kfs + Ap	Coe Coe + Phe	Ab, Qtz or mineral inclusion–free
Bt-bearing orthogneiss	Qtz Qtz + Ap	Coe + Ky Coe + Phe Coe + Ap Coe + Ky + Ap Coe + Ky + Ttn	Mineral inclusion–free

in zircons from sample B525 (Fig. 10). Neither coesite nor jadeite occurs in the matrix of the gneisses. The distribution of the UHP inclusions indicates that they are controlled not only on the P-T conditions, but also by the host-rock compositions (Liu et al., 2002).

Coesite and quartz inclusions commonly occur in different domains of single zircon grains (Figs. 10A–10D and Figs. 11A–11B). For example, zircons from samples B525 and B13 contain quartz inclusions in both cores (Figs. 10A, 10C, and Fig. 11A) and rims (Fig. 10A), whereas coesite inclusions are restricted to the mantles (Figs. 10A, 10C, 11A). As with other zoned grains, these zircons have low-luminescent cores surrounded by relatively bright-luminescent mantles, and low-luminescent rims (Figs. 10B, 10D, 11B).

A few zircon grains show different inclusion distributions. For example, some grains contain assemblages of Coe + Grt (Fig. 10E), Coe + Jd + Phe + Ap (Fig. 11C), and Coe + Grt + Ap (Fig. 11E) in both the core and mantle, whereas the rim is inclusion free (Figs. 10E, 10F, 11C–11F). In these grains, both cores and mantles have high luminescence and lack a clear boundary between them (Fig. 10F; Figs. 11D and 11F), indicating initial growth during the UHP stage or that these sections do not cut any inherited zircon cores.

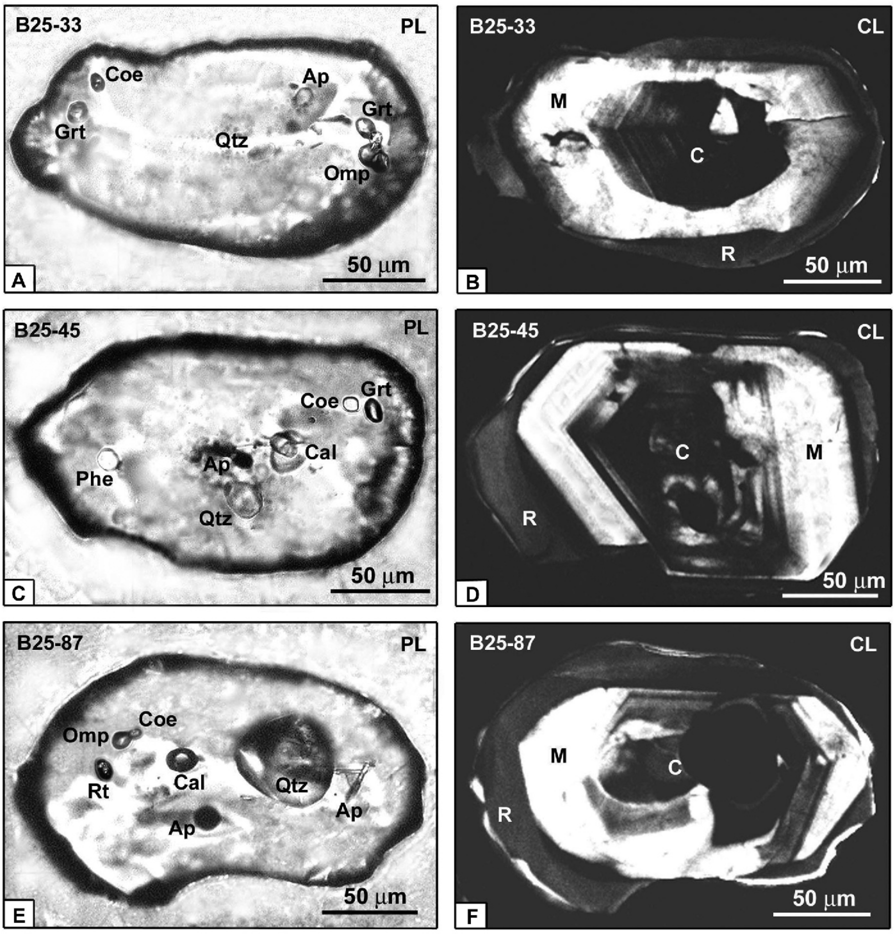

FIG. 9. Plane-polarized light (PL) images of mineral inclusion assemblages and CL images of host zircon from amphibolite (sample B25, 142.6 m depth). A. Zircon grain B25-33 showing Qtz + Ap inclusions in the core, Coe + Grt + Omp inclusions in the mantle, and an inclusion-free rim. B. CL image of the same zircon as in Figure 9A. Abbreviations: C = core; M= mantle; R = rim. C. Zircon grain B25-45 contains Qtz + Cal + Ap in the core, Coe + Grt + Phe in the mantle, and has an inclusion-free rim. D. CL image of the same zircon as in Figure 9C. E. Zircon grain B25-87 contains inclusions of Qtz + Cal + Ap in the core, Coe + Omp + Rt in the mantle, and has an inclusion-free rim. F. CL image of the same zircon as in Figure 9E shows bright luminescent core (C) and mantle (M), and low luminescent rim (R).

Mineral Inclusions in Zircon Separates from Orthogneiss

Zircons were separated from 159 samples from the CCSD-MH, and 56 of these contain coesite-bearing UHP inclusions in overgrowth domains (Fig. 2). Zircons from two representative samples, including epidote- and biotite-bearing granitic gneiss (B2487, 4809.1 m depth) and biotite-bearing granitic gneiss (B1811, 3623.6 m depth) were investigated in detail. The distribution of inclusions identified by laser Raman in these rocks is given in Table 1.

Mineral inclusions in zircon separates from the epidote- and biotite-bearing granitic gneiss

Both dusty and clear zircons occur in the epidote- and biotite-bearing gneiss, and both varieties contain coesite inclusions (Fig. 12, Table 1). The dusty zircons preserve inclusions in their cores and mantles (Figs. 12A and 12C). Those in the zircon cores consist mainly of Qtz + Ap (Fig. 12A) and Qtz + Kfs + Ap (Fig. 12C), whereas those in the mantles

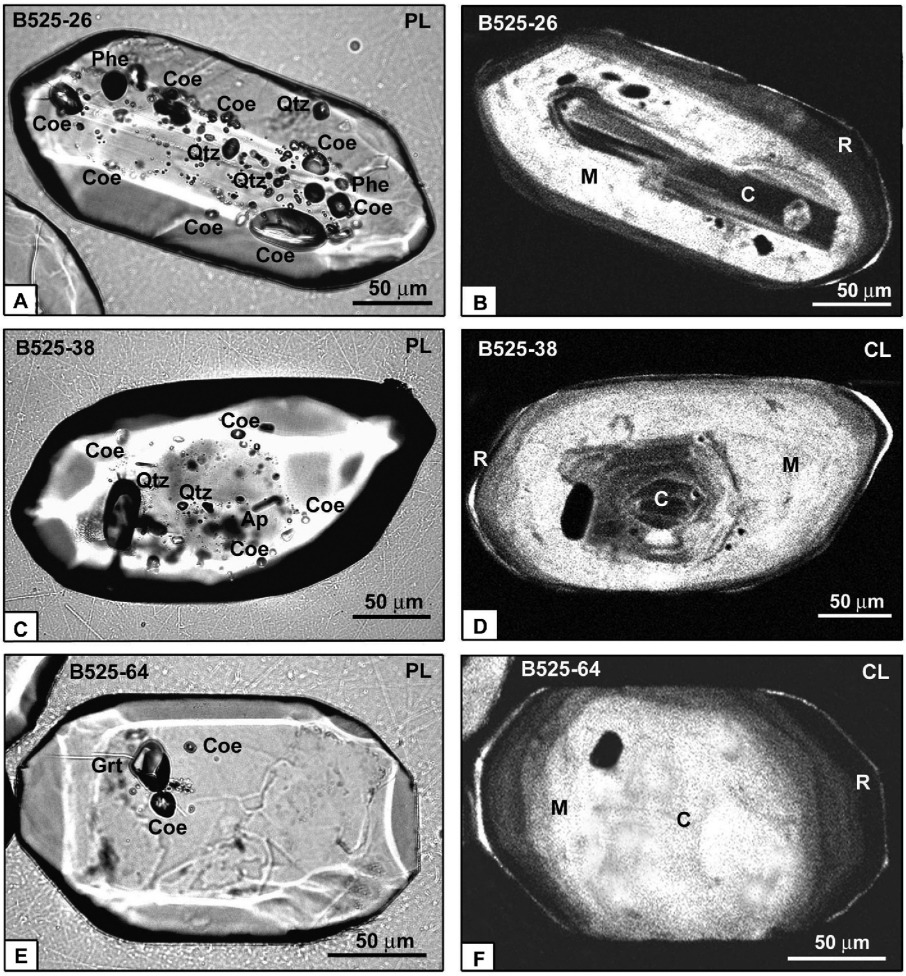

FIG. 10. Plane-polarized light (PL) images of mineral inclusions in zircons and CL images of host zircons from garnet-epidote-biotite-K-feldspar gneiss (B525, 958.7 m depth). A. Zircon grain B525-26 from B525 sample contains Qtz in the core, Coe + Phe in the mantle, and Qtz in the rim. B. CL image of the same zircon as in Figure 10A shows core (C), mantle (M), and rim (R) relationship. C. Zircon grain B525-38 from sample B525 contains Qtz + Ap in the core, Coe in the mantle, and has an inclusion-free rim. D. CL image of the same zircon as in Figure 10C shows core (C), mantle (M), and rim (R) relationship. E. Zircon grain B525-64 from sample B525 contains Coe + Grt inclusions in the core and mantle, and has an inclusion-free rim. F. CL image of the same zircon as in Figure 10E shows core (C), mantle (M), and rim (R) relationship.

are characterized by Coe (Fig. 12A) and Coe + Phe (Fig. 12C). The outmost rims are nearly free of inclusion (Figs. 12A and 12C); only a few contain Qtz or Ab (Table 1). The CL images reveal distinct zoning in these grains with low-luminescent cores surrounded by bright-luminescent mantles and low-luminescent rims (Figs. 12B and 12D). Most zircon cores are euhedral, preserve pronounced oscillatory zoning, and are considered to be igneous in origin.

Coesite inclusions were also identified in a few clear zircon grains from the same orthogneiss (Figs. 12E and 12F). The clear zircons are slightly smaller (40–150 μm) than the dusty grains (200–400 μm) and contain fewer inclusions. Identified inclusions include small ovoid grains of coesite in the cores and mantles and quartz in the rims (Fig. 12E). The grains all have bright-luminescent cores and mantle, surrounded by low-luminescent rims (Fig. 12F).

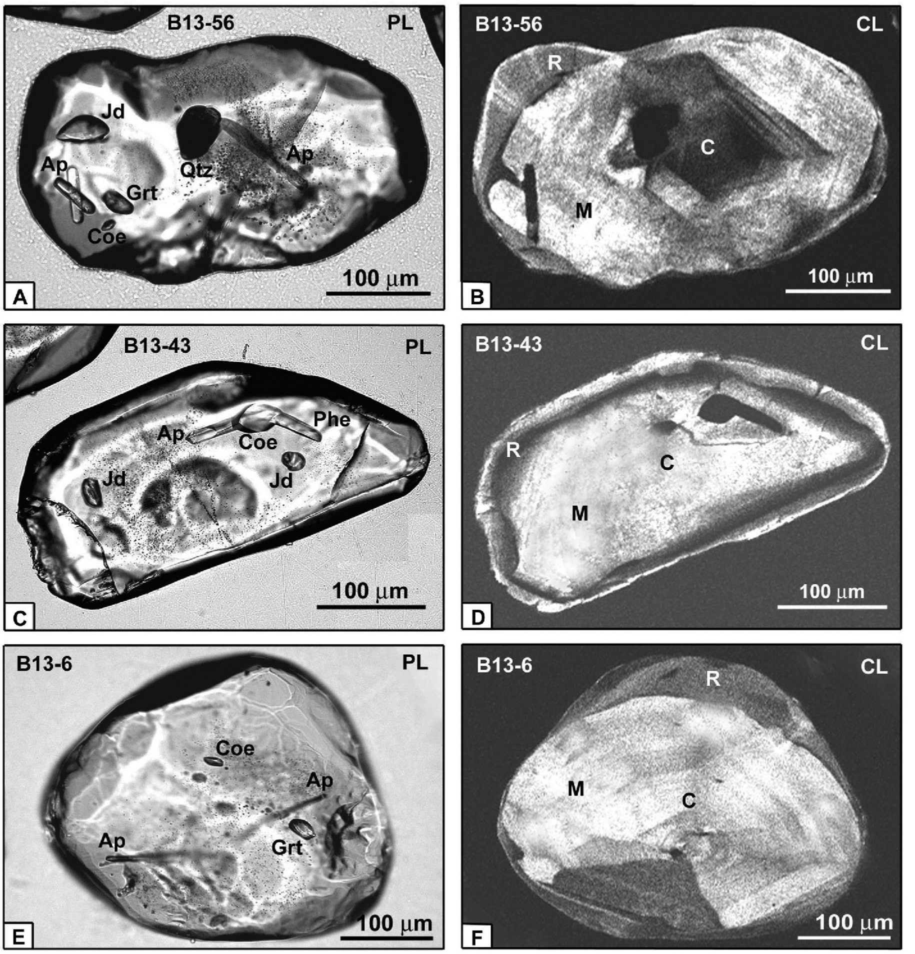

FIG. 11. Plane-polarized light (PL) images of mineral inclusions in zircons and CL images of host zircons from garnet-biotite-hornblende paragneiss (B13, 124.6 m depth). A. Zircon grain B13-56 from sample B13 contains Qtz + Ap inclusions in the core, and Coe + Grt + Jd + Ap in the mantle. B. CL image of the same zircon as in Figure 11A shows core (C), mantle (M), and rim (R) relationship. C. Zircon grain B13-43 from sample B13 contains Coe + Jd + Phe + Ap inclusions in the core and mantle. D. CL image of the same zircon as in Figure 11C shows core (C), mantle (M), and rim (R) relationship. E. Zircon grain B13-6 from sample B13 contains Coe + Grt + Ap inclusions in the core and mantle. F. CL image of the same zircon as in Figure 11E shows core (C), mantle (M), and rim (R) relationship.

These observations suggest that the clear zircons probably crystallized during UHP metamorphism, but we do not rule out the possibility that no cores were intersected in these sections.

Mineral inclusions in zircon separates from biotite-bearing granitic gneiss

Only dusty zircons were identified from biotite-bearing granitic gneiss (B1811, 3623.6 m depth); most zircon crystals separated from this sample contain abundant mineral inclusions, including coesite, kyanite, phengite, titanite, quartz, and apatite (Fig. 13, Table 1). The dusty zircons are anhedral to subhedral, and have low-luminescent cores surrounded by bright-luminescent mantles and low-luminescent rims (Fig. 13B). The cores (C) are euhedral, well zoned (Fig. 13B), and have inclusions of Qtz (Fig. 13F) and Qtz + Ap (Figs. 13A, 13C–13E), indicating that they are inherited magmatic grains. Numerous UHP mineral assemblages are present in the

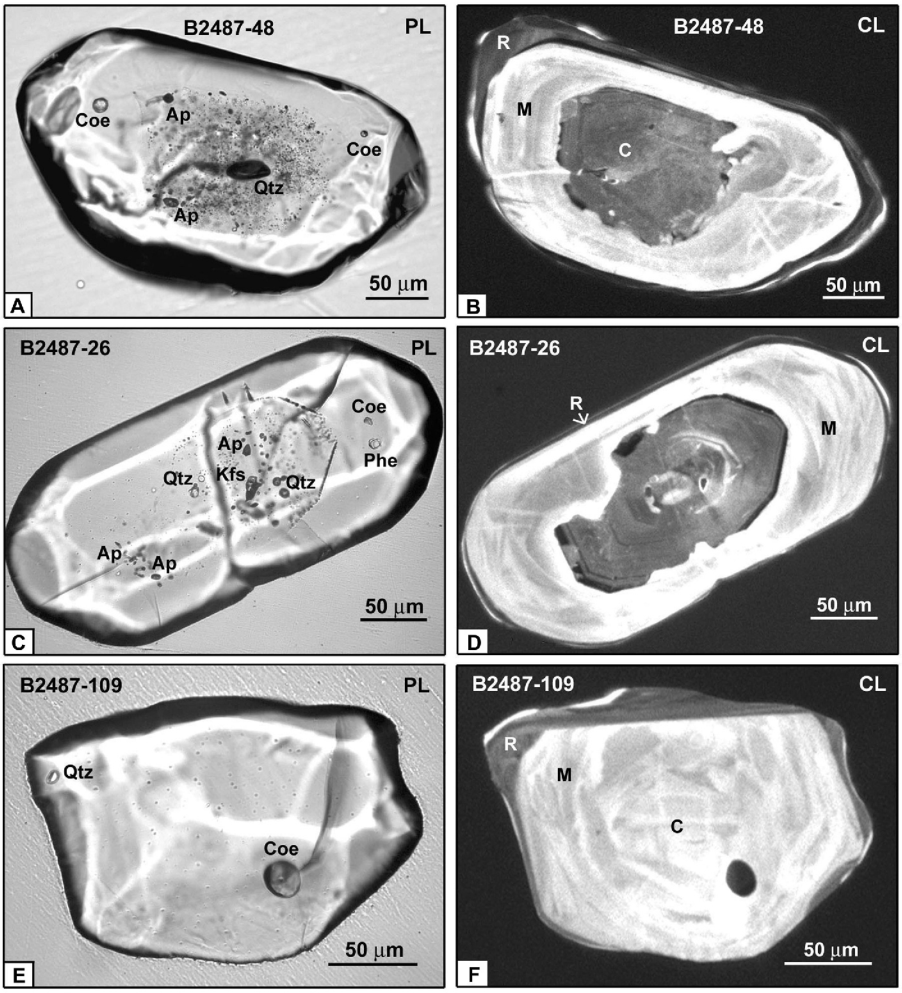

FIG. 12. Plane-polarized light (PL) images of mineral inclusions in zircons and CL images of host zircons from epidote- and biotite-bearing granitic gneiss (B2487, 4809.1 m depth). A. Zircon grain B2487-48 from sample B2487 contains Qtz + Ap in the core, Coe in the mantle, and has an inclusion-free rim. B. CL image of the same zircon as in Figure 12A shows core (C), mantle (M), and rim (R) relationship. C. Zircon grain B2487-26 from sample B2487 contains Qtz + Kfs + Ap in the core, Coe + Phe in the mantle, and has an inclusion-free rim. D. CL image of the same zircon as in Figure 12C shows core (C), mantle (M), and rim (R) relationship. E. Zircon grain B2487-109 from sample B2487 contains Coe inclusions in the core and mantle, and Qtz inclusion in the rim. F. CL image of the same zircon as in Figure 12E shows core (C), mantle (M), and rim (R) relationship.

metamorphic mantles, including Coe + Ky (Fig. 13A), Coe + Phe (Fig. 13C), Coe + Ap (Fig. 13D), Coe + Ky + Ap (Fig. 13E), and Coe + Ky + Ttn (Fig. 13F). The low-luminescent rims are inclusion free (Fig. 13B) and have CL images similar to those of retrograde zircon rims from the epidote- and biotite-bearing granitic gneiss (Figs. 12B and 12D). These zircons are interpreted as having a magmatic core, a UHP metamorphic mantle, and a retrograde rim.

Characteristic Raman Spectra of Index Inclusions in Zircons

Most of the coesite inclusions preserved in the zircons from eclogite, amphibolite, paragneiss, and orthogneiss are ovoid, and range from 2–25 μm in diameter (Figs. 8–13). They have a characteristic Raman spectrum at 524 cm^{-1} with weak peaks at 272 cm^{-1}, 181 cm^{-1}, and 124 cm^{-1} (Fig. 14A).

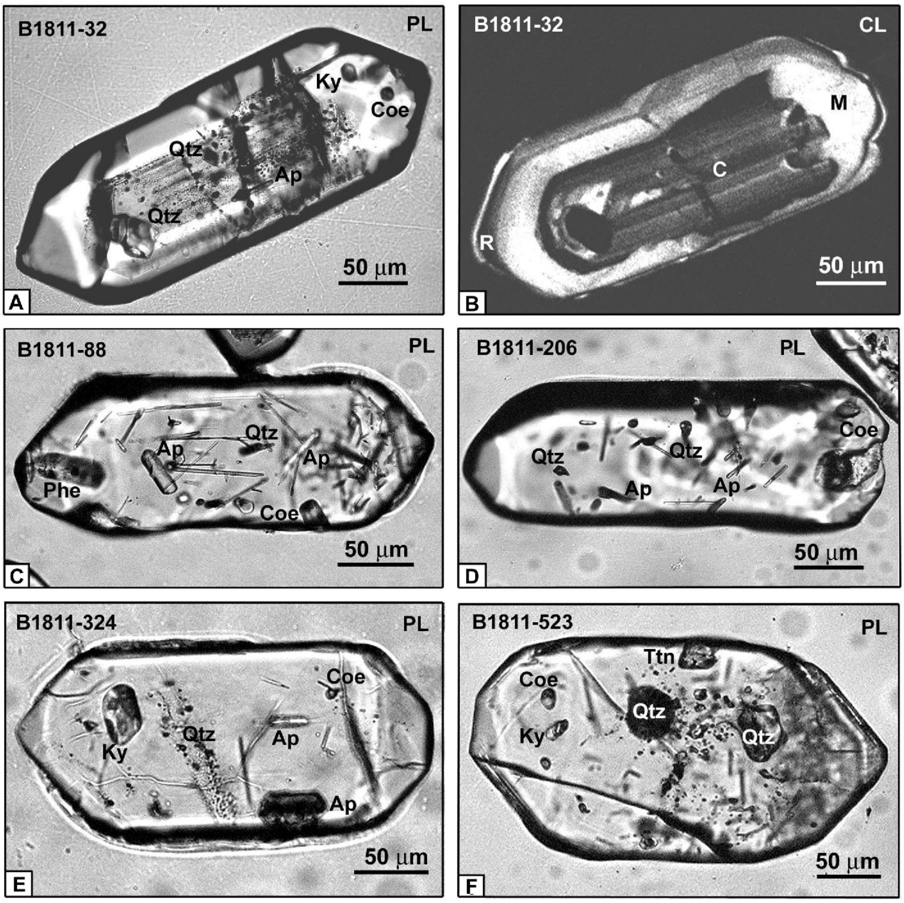

FIG. 13. Plane-polarized light (PL) images of mineral inclusions in zircons and CL images of host zircons from biotite-bearing granitic gneiss (B1811, 3623.6 m depth). A. Zircon grain B1811-32 from sample B1811 contains Qtz + Ap in the core and Coe + Ky in the mantle. B. CL image of the same zircon as in Figure 13A shows core (C), mantle (M), and rim (R) relationship. C. Zircon grain B1811-88 from sample B1811 contains Qtz + Ap in the core and Coe + Phe in the mantle. D. Zircon grain B1811-206 from sample B1811 contains Qtz + Ap in the core and Coe in the mantle. E. Zircon grain B1811-324 from sample B1811 contains Qtz + Ap in the core and Coe + Ky + Ap in the mantle. F. Zircon grain B1811-523 from sample B1811 contains quartz in the core and Coe + Ky + Ttn in the mantle.

Quartz inclusions in the zircon cores and rims, which were identified in all coesite-bearing samples, have a characteristic Raman peak at 466 cm^{-1} with a weak peak at 131 cm^{-1} (Fig. 14B), whereas jadeite inclusions (Figs. 11A and 11C) have a characteristic Raman band at 699 cm^{-1} with weak peaks at 574 cm^{-1} and 524 cm^{-1} (Fig. 14C). The sparse omphacite inclusions, associated with coesite in the zircons (Figs. 8E, 9A, and 9E) are characterized by a Raman peak at 688 cm^{-1} with a weak peak at 275 cm^{-1} (Fig. 14D). Garnet inclusions, which occur with coesite, omphacite, or jadeite (Figs. 8A, 8E, 9A, 9C, 10E, 11A, and 11C), were identified by a characteristic Raman peak at 906 cm^{-1} with weak peaks at 642 cm^{-1}, 559 cm^{-1}, and 506 cm^{-1} (Fig. 14E). The Raman spectrum for phengite, which occurs together with coesite both in zircon and in the country rocks, is characterized by peaks at 705 cm^{-1} and 264 cm^{-1} (Fig. 14F). Kyanite inclusions, together with coesite, were only identified in zircons from orthogneiss (Figs. 13A, 13E, and 13F) and are characterized by Raman peaks at 488 cm^{-1}, 405 cm^{-1}, and 302 cm^{-1} (Fig. 14G), whereas apatite is recognized by a characteristic peak at 965 cm^{-1} with a weak peak at 595 cm^{-1} (Fig. 14H).

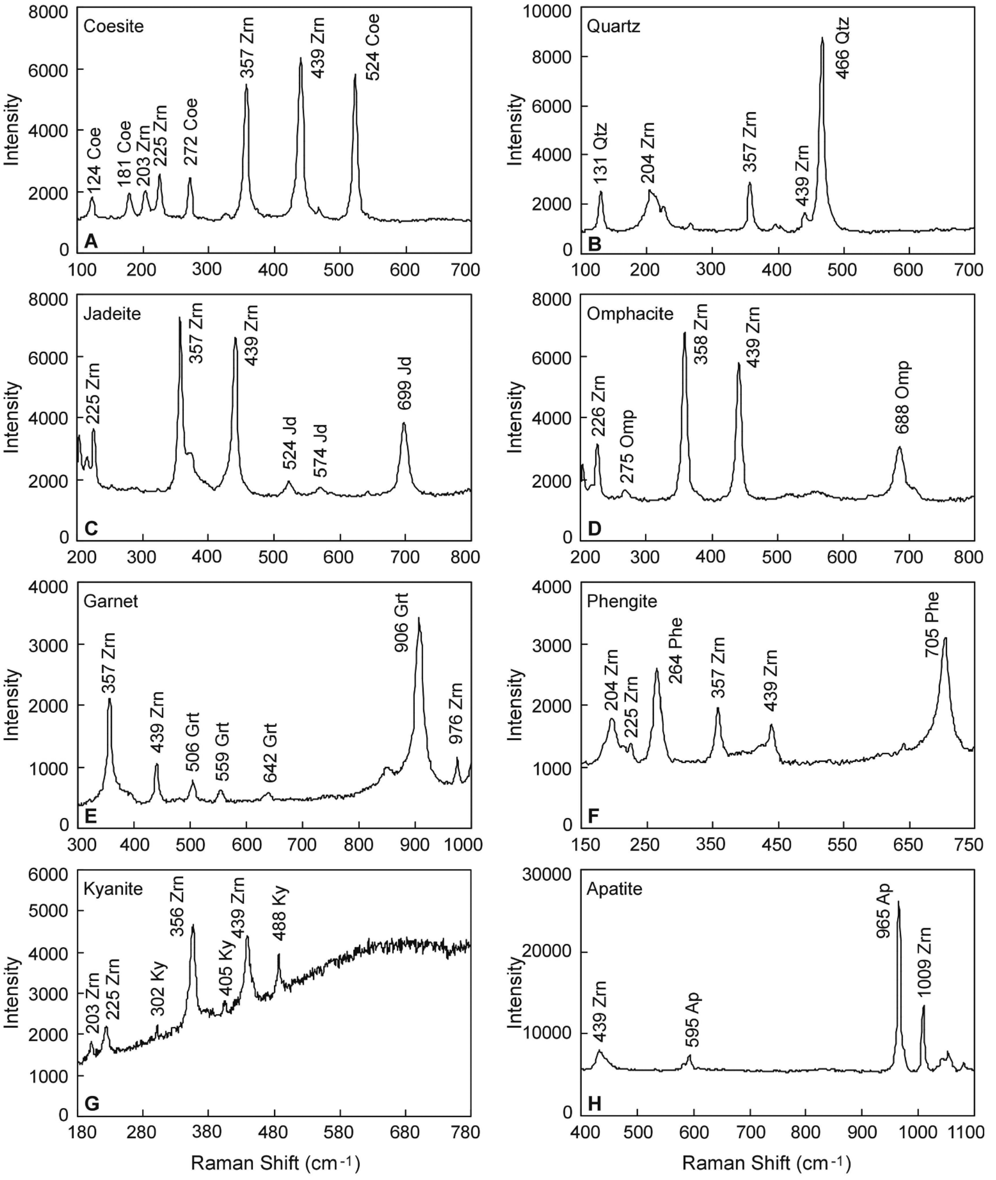

FIG. 14. Representative Raman spectra of minerals as inclusions in zircons from eclogite, amphibolite, paragneiss, and orthogneiss samples from the CCSD-MH. A. Coesite. B. Quartz. C. Jadeite. D. Omphacite. E. Garnet. F. Phengite. G. Kyanite. H. Apatite. These spectra also contain host zircon peaks at 203-204 cm^{-1}, 356-358 cm^{-1}, 439 cm^{-1}, 976 cm^{-1}, and 1009 cm^{-1}.

Chemical Compositions of Inclusions in Zircons from Eclogite and its Country Rocks

Representative analyses of mineral inclusions in zircons from eclogite and its country rocks are listed in Table 2.

Garnet

Garnet inclusions ($Alm_{42\text{-}43}Prp_{27\text{-}30}Sps_1Grs_{27\text{-}29}$) in coesite-bearing zircon from eclogite are low in MnO but have similar FeO, MgO, MnO, and CaO contents to matrix garnets ($Alm_{42\text{-}45}Prp_{26\text{-}28}Sps_1Grs_{28\text{-}29}$) from the same sample (Table 2, Fig.

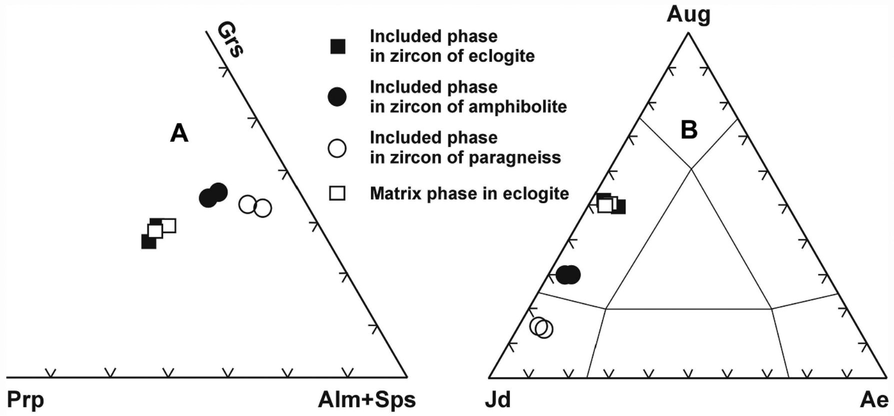

FIG. 15. Compositions of garnet, omphacite, and jadeite in zircons of eclogite, amphibolite, and paragneiss, and in matrix of eclogite from the CCSD-MH. A. Garnet. B. Omphacite and jadeite.

15A). Garnets from coesite-bearing domains in amphibolite ($Alm_{47-50}Prp_{13-17}Sps_{1-2}Grs_{34-36}$) have slightly higher FeO and CaO, and notably lower MgO contents than those from the eclogites (Table 2, Fig. 15A). Those from the paragneiss ($Alm_{52-54}Prp_{8-10}Sps_5Grs_{33}$) have the highest FeO and MnO but lowest MgO contents of any of the garnets analyzed (Table 2,; Fig. 15A). These compositional differences indicate that the garnet compositions are strongly controlled by bulk-rock chemistry. All of the garnet inclusions in zircons and in the matrix are homogeneous from core to the rim.

Omphacite

Clinopyroxene inclusions that occur with coesite and garnet in zircon from eclogite and amphibolite (Table 2) have omphacite compositions (Fig. 15B). Omphacite inclusions in zircons from amphibolite ($Jd_{66-67}Ae_{3-4}Aug_{30}$) have higher jadeite but lower augite components (Table 2, Fig. 15B) than similar inclusions in zircons ($Jd_{43-47}Ae_{1-8}Aug_{49-52}$) or omphacite grains from the matrix of eclogites ($Jd_{44-46}Ae_{3-5}Aug_{51}$). These variations also reflect differences in bulk-rock composition.

Jadeite

Compositions of Na-clinopyroxene inclusions in coesite-bearing zircon domains from paragneiss fall within the jadeite compositional field (Table 2, Fig. 15B). Compared with the compositions of omphacite inclusions in zircons ($Jd_{43-47}Ae_{1-8}Aug_{49-52}$) and matrix omphacite ($Jd_{44-46}Ae_{3-5}Aug_{51}$) from eclogite, these clinopyroxenes (Jd_{79-80} Ae_{6-8} Aug_{13-14}) are characterized by higher jadeite and lower augite contents, and are nearly free of Ti, Cr, Mn, and K. These compositions are similar to jadeite inclusions in zircons from paragneisses of drill hole CCSD-PP2 in Maobei (Liu et al., 2002), and to matrix jadeites from UHP jadeite-quartzite in Donghai (Zhang et al., 1995) and from Shuanghe in Dabie (Cong et al., 1995; Liou et al., 1997).

Phengite

Representative compositions of phengite inclusions are listed in Table 2. Those that occur with coesite in the same zircon domain have high Si values ranging from 3.384 to 3.435 p.f.u. in amphibolite, 3.415 to 3.424 p.f.u. in eclogite, and 3.428 to 3.453 p.f.u. (O = 11) in paragneiss. They are similar in composition to the matrix phengites in eclogite cores (Si = 3.446–3.460 p.f.u.; O = 11). Muscovite inclusions in the cores of zircon grains from eclogite (Fig. 8A) have lower Si values ranging from 3.124 to 3.236 p.f.u. (O = 11).

P-T Paths Indicated by Inclusions in Zircons from Eclogite, Amphibolite, and Paragneiss

Mineral inclusion assemblages and their distributions in different zircon domains from eclogite, amphibolite, paragneiss, and orthogneiss are shown in Table 1. Figures 8–13 indicate that the eclogite and its country rocks from the CCSD-MH have experienced multistage metamorphic recrystallization. P-T conditions for different stages of recrystallization were estimated by various geothermometers, geobarometers, thermochemical calculations, and

TABLE 2. Representative Compositions of Mineral Inclusions in Zircons and Minerals in Matrix of Eclogite, Amphibolite, and Paragneiss Cores in the Main Drill Hole of the Chinese Continental Scientific Drilling Project[1]

S. N.:	B42											
S. D.:	174.2 m											
Mineral:	Grt	Omp	Phe	Grt	Omp	Phe	Grt	Omp	Phe	Grt	Omp	Phe
Texture:	Z (Coe)	Z (Coe)	Z (Coe)	Z (Coe)	Z (Coe)	Z (Coe)	Max.	Mtx.	Mtx.	Mtx.	Mtx.	Mtx.
SiO_2	38.44	55.78	51.88	38.41	56.18	51.76	38.36	56.06	51.79	39.07	55.82	52.40
TiO_2	0.00	0.05	0.44	0.02	0.05	0.46	0.03	0.02	0.37	0.00	0.07	0.40
Al_2O_3	21.88	10.16	27.07	22.05	10.73	27.14	22.80	10.42	27.02	22.57	10.22	26.93
Cr_2O_3	0.09	0.01	0.38	0.01	0.00	0.33	0.01	0.09	0.21	0.01	0.03	0.01
FeO	21.00	5.71	2.28	20.59	4.35	2.18	21.02	4.68	2.24	19.94	5.14	2.49
MgO	8.09	7.46	3.66	7.08	8.57	3.74	6.77	8.70	3.69	7.38	8.77	3.71
MnO	0.39	0.08	0.01	0.43	0.00	0.02	0.49	0.00	0.01	0.32	0.00	0.13
CaO	9.92	12.77	0.09	10.56	12.93	0.07	10.28	12.85	0.05	10.40	12.65	0.00
Na_2O	0.02	7.31	0.70	0.03	6.66	0.64	0.05	6.72	0.54	0.03	6.83	0.36
K_2O	0.00	0.00	9.09	0.00	0.00	9.47	0.00	0.00	9.69	0.00	0.00	9.11
Total	99.83	99.33	95.60	99.63	99.47	95.81	99.81	99.54	95.61	99.72	99.53	95.54
O. N.	12	6	11	12	6	11	12	6	11	12	6	11
Si	2.952	1.999	3.424	2.953	2.006	3.415	2.947	2.000	3.428	2.984	1.992	3.453
Ti	0.000	0.001	0.022	0.001	0.001	0.023	0.002	0.001	0.018	0.000	0.002	0.020
Al	1.981	0.429	2.106	2.039	0.451	2.110	2.065	0.438	2.105	2.031	0.429	2.092
Cr	0.005	0.000	0.020	0.001	0.000	0.017	0.001	0.003	0.011	0.001	0.001	0.001
Fe^{3+}	0.000	0.078	0.000	0.000	0.000	0.000	0.000	0.023	0.000	0.000	0.055	0.000
Fe^{2+}	1.349	0.093	0.126	1.324	0.130	0.121	1.351	0.117	0.124	1.273	0.099	0.137
Mg	0.926	0.398	0.360	0.811	0.456	0.368	0.775	0.463	0.363	0.840	0.466	0.364
Mn	0.025	0.002	0.001	0.028	0.000	0.001	0.032	0.000	0.001	0.021	0.000	0.008
Ca	0.816	0.490	0.007	0.870	0.495	0.005	0.846	0.491	0.004	0.851	0.484	0.000
Na	0.001	0.508	0.089	0.001	0.461	0.082	0.002	0.465	0.069	0.002	0.472	0.046
K	0.000	0.000	0.766	0.000	0.000	0.797	0.000	0.000	0.817	0.000	0.000	0.766
Alm	42			43			45			42		
Prp	30			27			26			28		
Sps	1			1			1			1		
Grs	27			29			28			29		
Jd		43			47			46			44	
Ae		8			1			3			5	
Aug		49			52			51			51	

Table continues

TABLE 2. *Continued*

S. N.:	B25						B13					
S. D.:	146.2 m						124.6 m					
Mineral:	Grt	Omp	Phe	Grt	Omp	Phe	Grt	Jd	Phe	Grt	Jd	Phe
Texture:	Z (Coe)	Z (Coe)	Z (Coe)	Z (Coe)	Z (Coe)	Z (Coe)	Z (Coe)	Z (Coe)	Z (Coe)	Z (Coe)	Z (Coe)	Z (Coe)
SiO_2	38.59	56.95	51.49	38.50	57.19	51.09	37.94	57.78	51.79	37.35	57.89	51.41
TiO_2	0.03	0.09	0.36	0.04	0.05	0.03	0.08	0.05	0.85	0.05	0.04	0.64
Al_2O_3	21.58	16.40	26.25	21.61	16.58	28.71	21.39	17.97	25.80	21.42	18.03	25.66
Cr_2O_3	0.00	0.00	0.02	0.02	0.00	0.00	0.00	0.00	0.01	0.00	0.02	0.03
FeO	22.78	3.71	2.70	22.11	3.87	2.64	24.46	4.94	3.57	23.94	4.75	3.74
MgO	3.38	4.23	3.69	4.41	4.21	2.83	2.11	2.97	3.03	2.46	2.90	3.24
MnO	0.65	0.04	0.02	0.72	0.00	0.00	2.09	0.13	0.01	2.08	0.20	0.02
CaO	12.67	7.55	0.00	12.48	7.37	0.00	11.92	4.28	0.00	11.91	4.06	0.00
Na_2O	0.03	10.38	0.51	0.02	10.56	0.38	0.00	11.77	0.25	0.02	12.03	0.24
K_2O	0.00	0.00	10.46	0.00	0.00	9.91	0.00	0.00	10.09	0.00	0.00	10.55
Total	99.72	99.36	95.51	99.91	99.83	95.59	99.99	99.89	95.40	99.63	99.92	95.53
O. N	12	6	11	12	6	11	12	6	11	12	6	11
Si	3.015	2.004	3.435	2.994	1.995	3.384	2.996	2.008	3.460	2.987	2.008	3.446
Ti	0.002	0.002	0.018	0.002	0.001	0.001	0.005	0.001	0.042	0.003	0.001	0.038
Al	1.987	0.680	2.064	1.980	0.682	2.238	1.991	0.736	2.037	1.998	0.737	2.027
Cr	0.000	0.000	0.001	0.001	0.000	0.000	0.000	0.000	0.001	0.000	0.001	0.001
Fe^{3+}	0.000	0.016	0.000	0.000	0.039	0.000	0.000	0.037	0.000	0.000	0.054	0.000
Fe^{2+}	1.488	0.094	0.151	1.438	0.074	0.146	1.615	0.106	0.200	1.584	0.084	0.220
Mg	0.394	0.222	0.367	0.511	0.219	0.280	0.248	0.154	0.301	0.290	0.150	0.324
Mn	0.043	0.043	0.001	0.047	0.000	0.000	0.140	0.004	0.001	0.139	0.006	0.001
Ca	1.061	0.273	0.000	1.040	0.275	0.000	1.009	0.159	0.000	1.010	0.151	0.000
Na	0.001	0.708	0.066	0.001	0.714	0.049	0.000	0.793	0.033	0.001	0.809	0.031
K	0.000	0.000	0.890	0.000	0.000	0.837	0.000	0.000	0.860	0.000	0.000	0.902
Alm	50			47			54			52		
Prp	13			17			8			10		
Sps	1			2			5			5		
Grs	36			34			33			33		
Jd		67			66			80			79	
Ae		3			4			6			8	
Aug		30			30			14			13	

[1]S. N. = sample number; S. D.= depth of selected sample; O. N. = oxygen number; Z (Coe) = composition of mineral inclusion in the coesite-bearing zircon domain; Mtx. = composition of mineral in the matrix; B42 = eclogite; B25 = amphibolite; B13 = garnet-biotite-hornblende paragneiss.

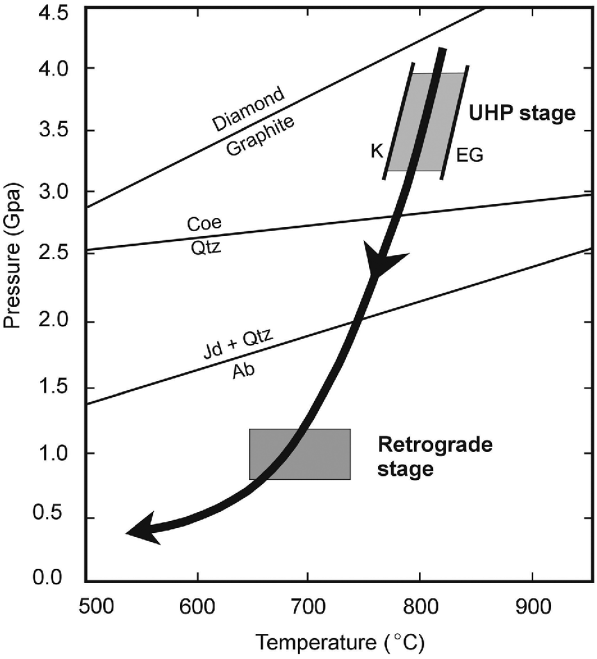

FIG. 16. P-T estimates for UHP and retrograde metamorphism based on inclusion assemblages in zircons and mineral assemblages in the matrix from eclogite, amphibolite, and paragneiss in the CCSD-MH. The equilibrium line for diamond = graphite is from Kennedy and Kennedy (1976); the line for Coe = Qtz is after Bohlen and Boettcher (1982); and the line for Jd + Qtz = Ab is from the GEO-CALC program of Berman (1988). K and EG represent the temperature estimates based on the garnet-clinopyroxene geothermometers calibrated by Krogh (1988) and Ellis and Green (1979), respectively.

established phase equilibria; the results are shown in Table 3, plotted in Figure 16, and described below.

UHP metamorphism

The UHP metamorphism produced assemblages of Coe + Grt + Omp (or Jd) and Coe + Grt + Omp (or Jd) + Phe in zircon domains from eclogite, amphibolite, and Grt-Bt-Hbl paragneiss (Table 1). Equilibrium temperatures for the UHP metamorphism were calculated using Fe-Mg exchange thermometers for coexisting garnet and clinopyroxene (including omphacite and jadeite) calibrated by Ellis and Green (1979), Krogh (1988), and Ravna (2000). Metamorphic pressures were calculated applying the Grt-Cpx-Phe barometer for coexisting garnet, omphacite (or jadeite), and phengite calibrated by Ravna and Terry (2004). Compositions for coexisting garnet, omphacite (or jadeite), and phengite inclusions in zircons from eclogite, amphibolite, and paragneiss yield similar temperature and pressure ranges (Table 3). The thermometer of Ellis and Green (1979) yields temperatures of 840–842°C for eclogite, 830–843°C for amphibolite, and 801–804°C for paragneiss, whereas the thermometer of Krogh (1988) yields temperatures of 815–819°C for eclogite, 806–817°C for amphibolite, and 773–775°C for paragneiss. Temperatures of 809–814°C for eclogite, 813-821°C for amphibolite, and 792–805°C for paragneiss were obtained using the thermometer of Ravna (2000). The geobarometer of Ravna and Terry (2004) yields metamorphic pressures of 3.2–3.3 GPa for eclogite, 3.6–3.8 GPa for amphibolite, and 3.5-4.0 GPa for paragneiss. These P-T estimates are similar to those of eclogite (T = 798–831°C, P = 3.1–3.3 GPa) calculated from the matrix minerals of eclogite from the CCSD-MH, using the same geothermometers and geobarometer (Table 3).

Retrograde metamorphism

Retrograde recrystallization is represented by the transformation of coesite-bearing mineral inclusions in zircon mantles to quartz-bearing inclusions

TABLE 3. Temperature and Pressure Estimates for UHP Metamorphism of Eclogite, Amphibolite, and Paragneiss from the Main Drill Hole of the Chinese Continental Scientific Drilling Project[1]

S. N.	R. T.	M. R.	Grt				Omp	
			Mg	Fe^{2+}	Ca	Mn	Mg	Fe^{2+}
B42	Ec.	Z (Coe)	0.926	1.349	0.816	0.025	0.398	0.093
	Ec.	Z (Coe)	0.811	1.324	0.870	0.028	0.459	0.110
	Ec.	Mtx.	0.775	1.351	0.846	0.032	0.463	0.117
	Ec.	Mtx.	0.840	1.273	0.851	0.021	0.466	0.099
B25	Amp.	Z (Coe)	0.394	1.488	1.061	0.043	0.222	0.094
	Amp.	Z (Coe)	0.511	1.438	1.040	0.047	0.219	0.074
B13	Para.	Z (Coe)	0.248	1.615	1.009	0.140	0.154	0.106
	Para.	Z (Coe)	0.290	1.584	1.010	0.139	0.150	0.084

S. N.	Phe		LnKd	P (GPa)	T_1 (°C)	T_2 (°C)	T_3 (°C)
	Mg	Fe^{2+}					
B42	0.360	0.126	1.8737	3.2	840	815	809
	0.368	0.121	1.9177	3.3	842	819	814
	0.363	0.124	1.9313	3.1	827	802	798
	0.364	0.137	1.9650	3.3	831	806	799
B25	0.367	0.151	2.1883	3.8	830	806	813
	0.280	0.146	2.1196	3.6	843	817	821
B13	0.301	0.200	2.2472	3.5	801	775	792
	0.324	0.220	2.2777	4.0	804	773	805

[1]S. N. = sample number; R. T. = rock type; M. R. = mineral pair selected for estimates of temperature and pressure; LnKd = $(Fe^{2+}/Mg)^{Grt}/(Fe^{2+}/Mg)^{Cpx}$; T_1 (°C), T_2 (°C), and T_3 (°C) = estimated temperature by garnet-clinopyroxene geothermometer of Ellis and Green (1979), Krogh (1988), and Ravna (2000), respectively; P (GPa) = estimated pressure by garnet-clinopyroxene-phengite geobarometer of Ravna and Terry (2004); Ec. = eclogite; Amp. = amphibolite; Para. = paragneiss; Z (Coe) = mineral inclusions in coesite-bearing zircon domain; Mtx. = minerals in matrix of eclogite.

in zircon rims (Table 1, Figs. 10A and 10B), and by the formation of albite in zircon rims (Table 1) within the stability field of albite (Fig. 16). It is difficult to calculate a temperature using only these retrograde minerals because there is no appropriate geothermometer. However, garnet and jadeite have been partly or completely replaced by a symplectite of fine-grained hornblende and sodic plagioclase in the matrix of eclogite and amphibolite (Fig. 3) and some garnet-bearing paragneisses from the CCSD-MH (Fig. 5), CCSD-PP2 (Liu et al., 2002), and outcrop samples in Donghai (Liu et al., 1999). Using coexisting hornblende and sodic plagioclase in these pseudomorphs, temperatures of 650–700°C are obtained using the Hbl-Pl thermometer of Blundy and Holland (1990). Coexisting hornblende and sodic plagioclase with relict garnet also yield similar temperatures of 660–720°C and pressures of 0.8–1.2 GPa using the Grt-Hbl-Pl-Qtz thermobarometer (Kohn and Spear, 1989). These estimates are consistent with temperatures of 650–720°C and pressures of 0.8–1.2 GPa for recrystallization of hornblende and plagioclase in eclogites (Enami et al., 1993; Zhang et al., 1995).

Discussion and Conclusions

It is well established that the country rocks of the Sulu-Dabie eclogites (e. g., amphibolite, paragneiss, and orthogneiss) experienced pronounced retrograde metamorphism, during which most UHP minerals were replaced by amphibolite-facies mineral assemblages (Figs. 3C, 3D, 4–7). Therefore, it is very difficult to identify relict UHP minerals in the matrix of the rocks hosting the eclogites. However, zircons separated from cores obtained from the CCSD-MH contain abundant index UHP mineral inclusions (e.g., coesite), indicating that both the eclogite and its surrounding rocks experienced UHP metamorphism. The presence of UHP mineral assemblages in zircons from core samples from the 5 km deep main hole indicates that the CCSD-MH did not penetrate through the Sulu UHP tectonic slice. Based on the attitude of the eclogite and its host rocks in the CCSD-MH (a NE-SW–trending foliation that dips 25–35° SE; Xu et al., 2004), the UHP slice has a minimum thickness of about 4500 m.

The unique mineral inclusion assemblages in zircons from a variety of UHP rocks in the CCSD-MH reflect bulk-rock compositions. For example, zircons from garnet-epidote-biotite–K-feldspar gneiss yield assemblages of Coe + Phe + Grt, whereas those from the garnet-biotite-hornblende paragneiss consist of Coe together with Jd + Grt + Phe + Ap. Zircons from the epidote- and biotite-bearing granitic gneiss contain inclusions of Coe + Phe and those from biotite-bearing granitic gneiss have Coe + Ky + Phe + Ttn + Ap. UHP inclusions in zircons from the biotite-epidote amphibolite consist mainly of Coe + Grt + Omp + Phe + Rt, which are very similar to those preserved in zircons from eclogite core samples. Clearly, the UHP inclusion assemblages are related not only to P-T conditions, but also to rock compositions.

The P-T estimates of UHP and retrograde metamorphism deduced from mineral inclusions in zircons and matrix phases from eclogite, amphibolite, and paragneiss are summarized in Table 3 and Figure 16. The UHP inclusion assemblages in zircons from eclogite and its country rocks record similar UHP metamorphic conditions at T = 773–843°C and P = 3.2–4.0 GPa, whereas the amphibolite-facies symplectites in the matrix of eclogite and its country-rocks record late retrograde metamorphism at T = 650–720°C and P = 0.8–1.2 GPa. These samples followed P-T paths similar to those of surface eclogites and jadeite-quartzites exposed in the southwest Sulu terrane (Enami et al., 1993; Zhang et al., 1995). Such consistency suggests that a coherent package of eclogite and its country rocks experienced coeval UHP metamorphism, and was then overprinted by amphibolite-facies retrograde metamorphism.

The size of the UHP slab provides a significant constraint on any subduction and exhumation model for the Sulu-Dabie terrane. Previous studies have identified coesite, quartz pseudomorphs after coesite, and other evidence of UHP metamorphism in eclogites from many Sulu-Dabie outcrops (Enami and Zang, 1989; Okay et al., 1989; Wang et al., 1989; Hirajima et al., 1990; Okay and Sengör, 1992; Zhang and Liou, 1994; Cong et al., 1995; Liou and Zhang, 1995, 1996; Carswell et al., 1996; Chavagnac and Jahn, 1996; Kato et al., 1997). Our studies show that coesite inclusions, along with other UHP minerals such as garnet, jadeite, omphacite, phengite, aragonite, kyanite, rutile, and titanite, are widespread in zircons from amphibolite-facies paragneiss, orthogneiss, marble, schist, quartzite, and amphibolite that crop out over approximately 5000 km^2 in the southwest Sulu terrane (Fig. 1; Liu et al., 2004a). Similar coesite inclusions have been found in 30 samples from the CCSD-PP1 (F.L. Liu et al., 2001) and 50 samples from CCSD-PP2 (Liu et al., 2002).

SHRIMP U-Pb dating of coesite-bearing zircon domains from one orthogneiss in the CCSD-MH and one paragneiss core in the CCSD-PP2 show metamorphic ages of 227 ± 2 Ma and 228 ± 5 Ma, respectively (Liu et al., 2004a, 2004b). Dated coesite-bearing zircon domains from eclogite and paragneiss in CCSD-MH record similar UHP metamorphic ages of 228 ± 3 Ma and 229 ± 4 Ma, respectively (Liu et al., 2006).

The distribution of UHP minerals in the CCSD-MH and the new age data cited above support our conclusion that both the eclogite and its host rocks experienced *in situ* UHP metamorphism. The rocks hosting eclogite are mainly granitic gneisses and metamorphosed passive-margin sedimentary rocks, including sandstone, shale, limestone, and minor mafic-ultramafic intrusive and extrusive rocks. These lines of evidences suggest that voluminous continental materials (area ≥ 5000 km^2, thickness ~4500 m) were subducted to mantle depths in excess of 100 km where they experienced UHP metamorphism. These UHP rocks were then rapidly exhumed to mid-crustal depth (the exhumation rate is about 5.0–6.0 km/Ma; Liu et al., 2004a, 2004b) and overprinted by Barrovian-type, amphibolite-facies metamorphism.

Acknowledgments

This study was supported in part by the National Natural Science Foundation of China (grant No.

40399143), the National 973 Project of the Chinese Ministry of Science and Technology (grant No. 2003CB716502), the Program of Excellent Young Scientists of the Ministry of Land and Resources of China and the CCSD. It also represents one of the research products for a Sino-American cooperative project supported by NSF EAR 0003355 and 0506901. The manuscript was critically reviewed and materially improved by Dr. K. Sajeev, Dr. I. Katayama, Prof. W. G. Ernst, Prof. P. Robinson, and an anonymous reviewer, and benefited from many discussions with Profs. Qihan Shen and Jingsui Yang.

REFERENCES

Berman, R. G., 1988, Internally-consistent thermodynamic data for minerals in the system Na_2O-K_2O-CaO-MgO-FeO-Fe_2O_3-Al_2O_3-SiO_2-H_2O-CO_2: Journal of Petrology, v. 29, p. 445–522.

Blundy, J. D., and Holland, T. J. B., 1990, Calcic amphibole-bearing equilibria and a new amphibole plagioclase geothermometer: Contributions to Mineralogy and Petrology, v. 104, p. 208–224.

Bohlen, S. R., and Boettcher, A. L., 1982, The quartz-coesite transformation: A pressure determination and the effects of other components: Journal of Geophysical Research, v. 104, p. 208–224.

Carswell, D. A., O'Brien, P. J., Wilson, R. N., and Zhai, M. G., 1996, Ultrahigh pressure aluminous titanites in carbonate-bearing eclogites at Shuanghe in Dabieshan, central China: Mineralogical Magazine, v. 60, p. 461–471.

Chavagnac, V., and Jahn, B.-M., 1996, Coesite-bearing eclogites from the Bixiling Complex, Dabie Mountains, China: Sm-Nd ages, geochemical characteristics, and tectonic implications: Chemical Geology, v. 133, p. 29–51.

Chopin, C., and Sobolev, N. V., 1995, Principal mineralogic indicators of UHP in crustal rocks, *in* Coleman, R. G., and Wang, X. M., eds., Ultrahigh pressure metamorphism: Cambridge, UK, Cambridge University Press, p. 96–131.

Cong, B. L., Zhai, M. G., Carswell, D. A., Wilson, R. N., Wang, Q. C., Zhao, Z., and Windley, B. F., 1995, Petrogenesis of the ultrahigh-pressure rocks and their country rocks at Shuanghe in Dabieshan, central China: European Journal of Mineralogy, v. 7, p. 119–138.

Ellis, D. J., and Green, D. H., 1979, An experimental study of the effect of Ca upon garnet-clinopyroxene Fe-Mg exchange equilibria: Contributions to Mineralogy and Petrology, v. 71, p. 13–22.

Enami, M., and Zang, Q. J., 1989, Quartz pseudomorph after coesite in eclogites from Shandong province, east China: American Mineralogist, v. 75, p. 381–386.

Enami, M., Zang, Q. J., and Yin, Y. J., 1993, High-pressure eclogites in north Jiangsu–southern Shandong province, east China: Journal of Metamorphic Geology, v. 11, p. 589–603.

Hacker, B. R., Ratschbacher, L., Webb, L., Ireland, T., Walker, D., and Dong, S., 1998, U/Pb zircon ages constrain the architecture of the ultrahigh-pressure Qinling-Dabie Orogen, China: Earth and Planetary Science Letters, v. 161, p. 215–230.

Hirajima, T., Ishiwatarri, A., Cong, B., Zhang, R. Y., Banno, S., and Nozaka, T., 1990, Coesite from Mengzhong eclogite at Donghai county, northeastern Jiangsu province, China: Mineralogical Magazine, v. 54, p. 579–583.

Katayama, I., Zayakhstan, A. A., and Maruyama, S., 2000, Progressive P-T records from zircon in Kokchetav UHP-HP rocks, northern Kazakhstan: The Island Arc, v. 9, p. 417–427.

Kato, T., Enami, A., and Zhai, M. G., 1997, Ultrahigh-pressure marble and eclogite in the Su-Lu UHP terrane, eastern China: Journal of Metamorphic Geology, v. 15, p. 169–182.

Kennedy, C. A., and Kennedy, G. C., 1976, The equilibrium boundary between graphite and diamond: Journal of Geophysical Research, v. 81, p. 2467–2470.

Kretz, R., 1983, Symbols for rock-forming minerals: American Mineralogist, v. 68, p. 277–279.

Kohn, M. J., and Spear, F. S., 1989, Empirical calibration of geobarometers for the assemblage garnet + hornblende + plagioclase + quartz: American Mineralogist, v. 74, p. 77–84.

Krogh, E. J., 1988, The garnet-clinopyroxene Fe-Mg geothermometer—a reinterpretation of existing experimental data: Contributions to Mineralogy and Petrology, v. 99, p. 44–48.

Liou, J. G., Hacker, B. R., and Zhang, R. Y., 2000, Into the forbidden zone: Science, v. 287, p. 1215–1216.

Liou, J. G., and Zhang, R. Y., 1995, Significance of ultrahigh-P talc-bearing eclogitic assemblages: Mineralogical Magazine, v. 59, p. 93–102.

Liou, J. G., and Zhang, R. Y., 1996, Occurrence of intergranular coesite in Sulu ultrahigh-P rock from China: Implications for fluid activity during exhumation: American Mineralogist, v. 81, p. 1217–1221.

Liou, J. G., Zhang, R. Y., and Jahn, B.-M., 1997, Petrology, geochemistry and isotope data on a ultrahigh-pressure jadeite quartzite from Shuanghe, Dabie mountains, east-central China: Lithos, v. 41, p. 59–78.

Liu, F. L., Xu, Z. Q., Katayama, I., Yang, J. S., Maruyama, S., and Liou, J. G., 2001, Mineral inclusions in zircons of para- and orthogneiss from pre-pilot drillhole CCSD-PP1, Chinese Continental Scientific Drilling Project: Lithos, v. 59, p. 199–215.

Liu, F. L., Xu, Z. Q., Liou, J. G., Katayama, I., Masago, H., Maruyama, S., and Yang, J. S., 2002, Ultrahigh-pressure mineral inclusions in zircons from gneissic core samples of the Chinese Continental Scientific Drilling

Site in eastern China: European Journal of Mineralogy, v. 14, p. 499–512.

Liu, F. L., Xu, Z. Q., Liou, J. G., and Song, B., 2004a, SHRIMP U-Pb ages of ultrahigh-pressure and retrograde metamorphism of gneisses, south-western Sulu terrane, eastern China: Journal of Metamorphic Geology, v. 22, p. 315–326.

Liu, F. L., Xu, Z. Q., Xu, H. F., and Yang, J. S., 1999, High- and ultrahigh-pressure metamorphism and retrogressive textures of gneiss in the Donghai area: Evidence from gneisses in drillhole ZK2304: Acta Geologica Sinica, v. 73, p. 300–315.

Liu, F. L., Xu, Z. Q., and Xue, H. M., 2004b, Tracing the protolith, UHP metamorphism, and exhumation ages of orthogneiss from the SW Sulu terrane (eastern China): SHRIMP U-Pb dating of mineral inclusion-bearing zircons: Lithos, v. 78, p. 411–429.

Liu, F. L., Xu, Z. Q., Xue, H. M., and Zhou, K. F., 2006, Ultrahigh-pressure and retrograde metamorphic ages for Paleozoic protolith of paragneiss in the main drill hole of the Chinese Continental Scientific Drilling Project (CCSD-MH), SW Sulu UHP terrane: Acta Geologica Sinica, v. 80, p. 336–348.

Liu, F. L., Zhang, Z. M., Katayama, I., Xu, Z. Q., and Maruyama, S., 2003, Ultrahigh-pressure metamorphic records hidden in zircons from amphibolites in Sulu terrane, eastern China: The Island Arc, v. 12, p. 256–267.

Liu, J. B., Ye, K., Maruyama, S., Cong, B. L., and Fan, H. R., 2001, Mineral inclusions in zircon from gneisses in the ultrahigh-pressure zone of the Dabie Mountains, China: Journal of Petrology, v. 109, p. 523–535.

Okay, A. I., and Sengör, A. M. C., 1992, Evidence for intra-continental thrust–related exhumation of the ultra-high pressure rocks in China: Geology, v. 20, p. 411–414.

Okay, A. I., Xu, S., and Sengör, A. M. C., 1989, Coesite from the Dabie Shan eclogites, central China: European Journal of Mineralogy, v. 1, p. 595–598.

Ravna, E. K., 2000, The garnet-clinopyroxene Fe^{2+}-Mg geothermometer: An updated calibration: Journal of Metamorphic Geology, v. 18, p. 211–219.

Ravna, E. K., and Terry, M. P., 2004, Geothermobarometry of UHP and HP eclogites and schists—an evaluation of equilibria among garnet-clinopyroxene-kyanite-phengite-coesite/quartz: Journal of Metamorphic Geology, v. 22, p. 579–592.

Tabata, H., Yamauchi, K., Maruyama, S., and Liou, J. G., 1998, Tracing the extent of a UHP metamorphic terrane: Mineral-inclusion study of zircons in gneisses from the Dabieshan, *in* Hacker, B. R., and Liou, J. G., eds., When continents collide: Geodynamics and geochemistry of ultrahigh-pressure rocks: Dordrecht, The Netherlands, Kluwer Academic Publishers, p. 261–273.

Wang, X. M., and Liou, J. G., 1991, Regional ultrahigh-pressure metamorphic terrane in central China: Evidence from coesite-bearing eclogite, marble and metapelite: Geology, v. 19, p. 933–936.

Wang, X. M., Liou, J. G., and Mao, H. G., 1989, Coesite-bearing eclogites from the Dabie Mountains in central China: Geology, v. 17, p. 1085–1088.

Xu, S., Liu, Y., Chen, G. B., Ji, S. Y., Ni, P., and Xiao, W. S., 2005, Microdiamonds, their classification, and tectonic implications for the host eclogites from the Dabie and Su-Lu regions in central eastern China: Mineralogical Magazine, v. 69, p. 509–520.

Xu, S., Okay, A. I., Ji, S., Sengör, A. M. C., Su, W., Liu, Y., and Jiang, L., 1992, Diamond from the Dabie Shan metamorphic rocks and its implication for tectonic setting: Science, v. 256, p. 80–82.

Xu, Z. Q., Zhang, Z. M., Liu, F. L., Yang, J. S., Li, H. B., Yang, T. N., Qiu, H. J., Li, T. F., Meng, F. C., Chen, S. Z., Tang, Z. M., and Chen, F. Y., 2003, Exhumation structure and mechanism of the Sulu ultrahigh-pressure metamorphic belt, central China: Acta Geologica Sinica, v. 77, p. 433–450 (in Chinese with English abstract).

Xu, Z. Q., Zhang, Z. M., Liu, F. L., Yang, J. S., Tang, Z. M., Chen, S. Z., Cai, Y. C., Li, T. F., and Chen, F. Y., 2004, The structure profile of 0–1200 m in the main borehole, Chinese Continental Scientific Drilling Project and its preliminary deformation analysis: Acta Petrologica Sinica, v. 20, p. 53–72 (in Chinese with English abstract).

Xu, Z. Q., Zeng, L. S., Liu, F. L., Yang, J. S., Zhang, Z. M., McWilliams, M., and Liou, J. G., 2006, Polyphase subduction and exhumation of the Sulu high-pressure–ultrahigh-pressure metamorphic terrane: Geological Society of America Special Paper, v. 403, p. 93–113.

Ye, K., Yao, Y., Katayama, I., Cong, B., Wang, Q., and Maruyama, S., 2000, Large areal extent of ultrahigh-pressure metamorphism in the Sulu ultrahigh-pressure terrane of eastern China: New implications from coesite and omphacite inclusions in zircon of granitic gneiss: Lithos, v. 52, p. 157–164.

Zhang, R. Y., Hirajima, T., Banno, S., Cong, B. L., and Liou, J. G., 1995, Petrology of ultrahigh-pressure rocks from the southern Sulu region, eastern China: Journal of Metamorphic Geology, v. 13, p. 659–675.

Zhang, R. Y., and Liou, J. G., 1994, Coesite-bearing eclogite in Henan Province, central China: Detailed petrology, glaucophane stability, and PT path: European Journal of Mineralogy, v. 6, p. 217–233.

Zhang, R. Y., Liou, J. G., and Shu, J. F., 2002, Hydroxyl-rich topaz in high-pressure and ultrahigh-pressure kyanite quartzite, with retrograde woodhouseite, from the Sulu terrane, eastern China: American Mineralogist, v. 87, p. 445–453.